Ten Lectures on Spatially Localized Structures

Edgar Knobloch

Department of Physics
University of California, Berkeley, CA 94720, USA
http://tardis.berkeley.edu

Imperial College, 23-27 May 2016

Density functional theory (DFT) and variants

The grand free energy of a system of interacting particles is

$$\Omega[\rho(\mathbf{r})] = k_B T \int d\mathbf{r}\rho(\mathbf{r})[\ln \Lambda^d \rho(\mathbf{r}) - 1] + \mathcal{F}_{ex}[\rho(\mathbf{r})] + \int d\mathbf{r}\,(\Phi(\mathbf{r}) - \mu)\rho(\mathbf{r}),$$

where $\mathcal{F}_{ex}[\rho(\mathbf{r})]$ is the excess free energy due to particle-particle interaction and $\Phi(\mathbf{r})$ is an external confining potential. When $\Phi = 0$ (the bulk case) $\Omega[\rho(\mathbf{r})]$ may be minimized by constant or nonconstant ρ, depending on the temperature T.

Near-equilibrium dynamics are described by dynamical density functional theory (DDFT):

$$\frac{\partial \rho(\mathbf{r}, t)}{\partial t} = \Gamma \nabla \cdot \left[\rho(\mathbf{r}, t) \nabla \frac{\delta \Omega[\rho(\mathbf{r}, t)]}{\delta \rho(\mathbf{r}, t)} \right],$$

where $\rho(\mathbf{r}, t)$ is now the time-dependent nonequilibrium one-body density profile and $\Gamma \equiv \beta D$ is the mobility. Here D is the diffusion coefficient and $\beta = (k_B T)^{-1}$. In deriving this equation we have used the equilibrium free energy functional $\mathcal{F} \equiv \mathcal{F}_{id} + \mathcal{F}_{ex}$ to approximate the unknown nonequilibrium free energy.

DDFT predictions generally agree well with studies of Brownian particles governed by

$$\dot{\mathbf{r}}_i = -\Gamma \nabla_i U(\{\mathbf{r}_i\}, t) + \Gamma \mathbf{X}_i(t),$$

where the index $i = 1, ..., N$ labels the particles,

$$U(\{\mathbf{r}_i\}, t) = \sum_{i=1}^{N} \Phi(\mathbf{r}_i) + \sum_{i \neq j} V(\mathbf{r}_i - \mathbf{r}_j)$$

is the potential energy of the system and $\mathbf{X}_i(t)$ is a white noise term. Simulations of this type of system are called Brownian dynamics simulations.

The DDFT model can be simplified further, resulting in the so-called Phase Field Crystal model (PFC). This model is characterized by an order parameter $\phi(\mathbf{r}) \propto \rho(\mathbf{r}) - \rho_0$, with $\phi = \text{const}$ identified with the liquid phase and $\phi \neq \text{const}$ identified with the solid phase.

The Phase Field Crystal model

The Phase Field Crystal (PFC) model is an approximation to Dynamical Density Functional Theory [Archer et al, PRE **86**, 031603 (2012)] and takes the form

$$\partial_t \phi(\mathbf{x}, t) = \alpha \nabla^2 \frac{\delta F[\phi]}{\delta \phi(\mathbf{x}, t)},$$

where $F[\phi]$ denotes the free energy functional

$$F[\phi] \equiv \int d\mathbf{x} \left[\frac{\phi}{2} [r + (q^2 + \nabla^2)^2] \phi + \frac{\phi^4}{4} \right],$$

$\phi(\mathbf{x}, t)$ is an order parameter field that corresponds to scaled density and α is a (constant) mobility coefficient. Here $\mathbf{x} = (x, y, z)$, $\nabla = (\partial_x, \partial_y, \partial_z)$. It follows that the system evolves according to the equation

$$\partial_t \, \phi \; = \; \alpha \nabla^2 \left[r\phi + (q^2 + \nabla^2)^2 \phi + \phi^3 \right].$$

i.e., the conserved Swift-Hohenberg equation (cSHE). In 1D this equation also describes stationary 2D binary fluid convection at positive separation ratios [Knobloch, PRA **40**, 1549 (1989)].

In one dimension, with $\alpha = 1$ and $q = 1$, we have

$$\partial_t \phi = \partial_x^2 \left[r\phi + (1 + \partial_x^2)^2 \phi + \phi^3 \right].$$

This equation is reversible in space (i.e., it is invariant under $x \to -x$). Moreover, it conserves the total "mass" $\int_0^L \phi \, dx$, where L is the size of the system. In the following we denote the average value of ϕ in the system by $\phi_0 \equiv \langle \phi \rangle$ so that perturbations $\tilde{\phi} \equiv \phi - \phi_0$ necessarily satisfy $\langle \tilde{\phi} \rangle = 0$, where $\langle \cdots \rangle \equiv L^{-1} \int_0^L (\cdots) \, dx$.
Linearizing about $\phi = \phi_0$ results in the dispersion relation

$$\sigma = -k^2 \left[r + (1 - k^2)^2 + 3\phi_0^2 \right],$$

and hence instability for $r < -3\phi_0^2$.

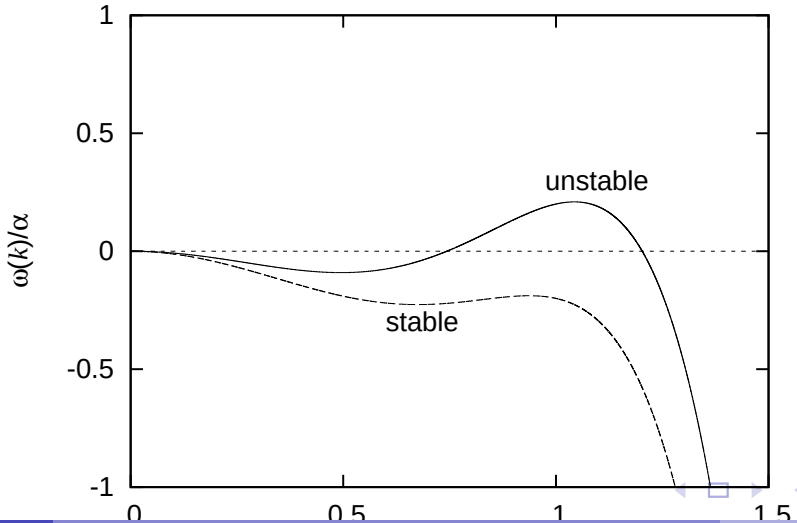

Steady states

Steady states ($\partial_t \phi = 0$) are solutions of the fourth order ordinary differential equation

$$0 = r\phi + (1 + d_x^2)^2 \phi + \phi^3 - \mu,$$

where μ is an integration constant that corresponds to the chemical potential. Each solution of this equation corresponds to a stationary value of F.

We use the free energy to define the grand potential

$$\Omega = \tilde{F} - \mu \int_0^L \phi \, dx$$

and are interested in the free energy density $f \equiv (\tilde{F}[\phi(x)] - \tilde{F}[\phi_0])/L$ and in the density of the grand potential $\omega \equiv \Omega/L = \tilde{F}[\phi(x)]/L - \mu\phi_0$.

We also use the L^2 norm

$$||\delta\phi|| = \sqrt{\frac{1}{L} \int_0^L (\phi - \phi_0)^2 \, dx}$$

The tricritical point

The thermodynamic tricritical point is located at

$$(\phi_{tcp}, r_{tcp}) = (\pm\sqrt{3/38}, -9/38)$$

[Archer et al, PRE **86**, 031603 (2012)]. For $r > r_{tcp}$ there exists no thermodynamic coexistence zone between the homogeneous and periodic states. Such a region is only present for $r < r_{tcp}$ and is limited by the binodal lines that indicate the values of ϕ_0 for which the homogeneous and periodic solutions at fixed r have equal chemical potential and pressure (i.e., equal grand potential). Thus for $r < r_{tcp}$ the transition from the homogeneous to the periodic state is of first order.

Remark: This is not the same as saying the bifurcation to the crystal state is subcritical.

The results that follow are from Thiele et al., PRE **87**, 042915 (2013).

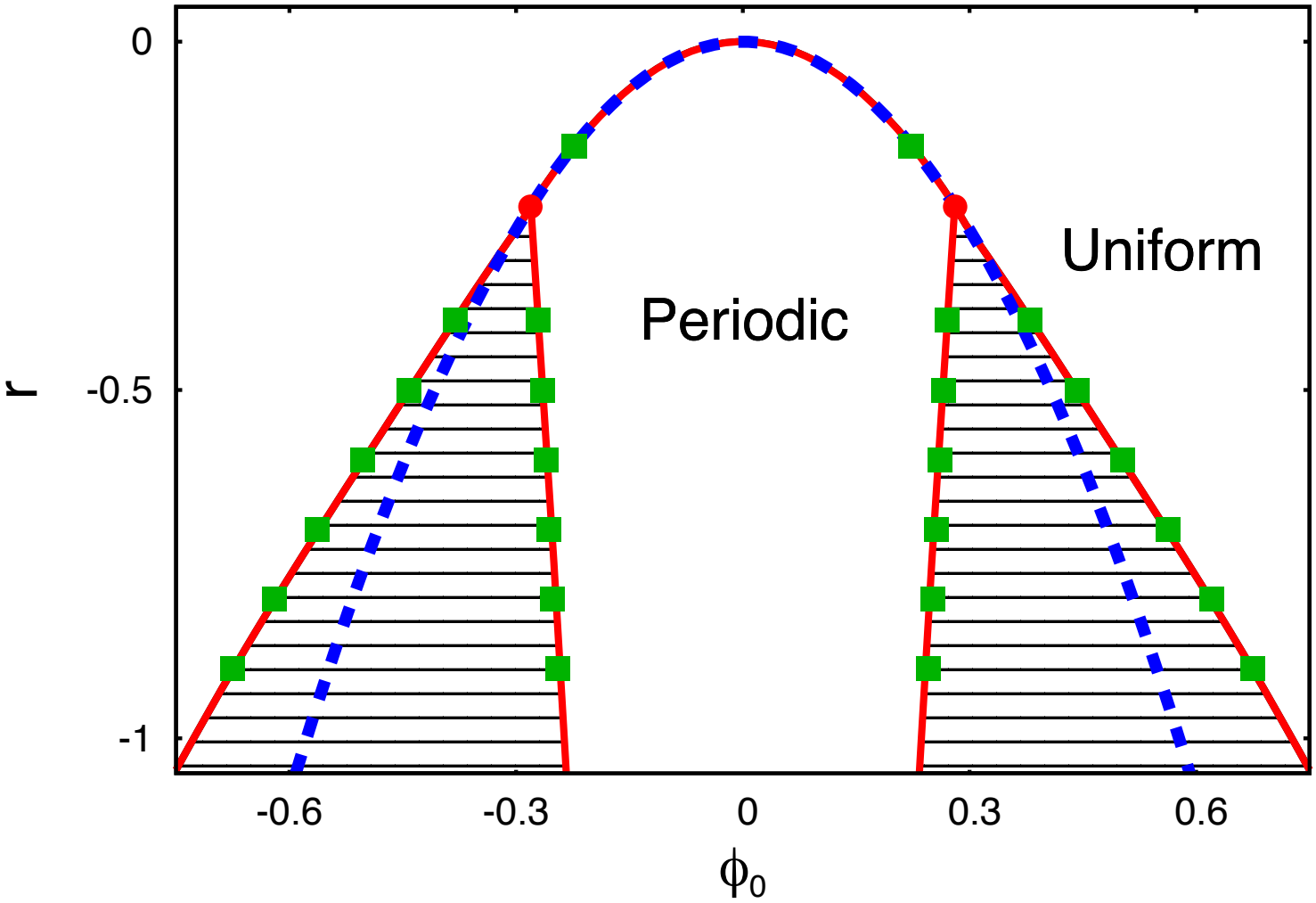

The phase diagram for the 1D PFC model when $q = 1$.

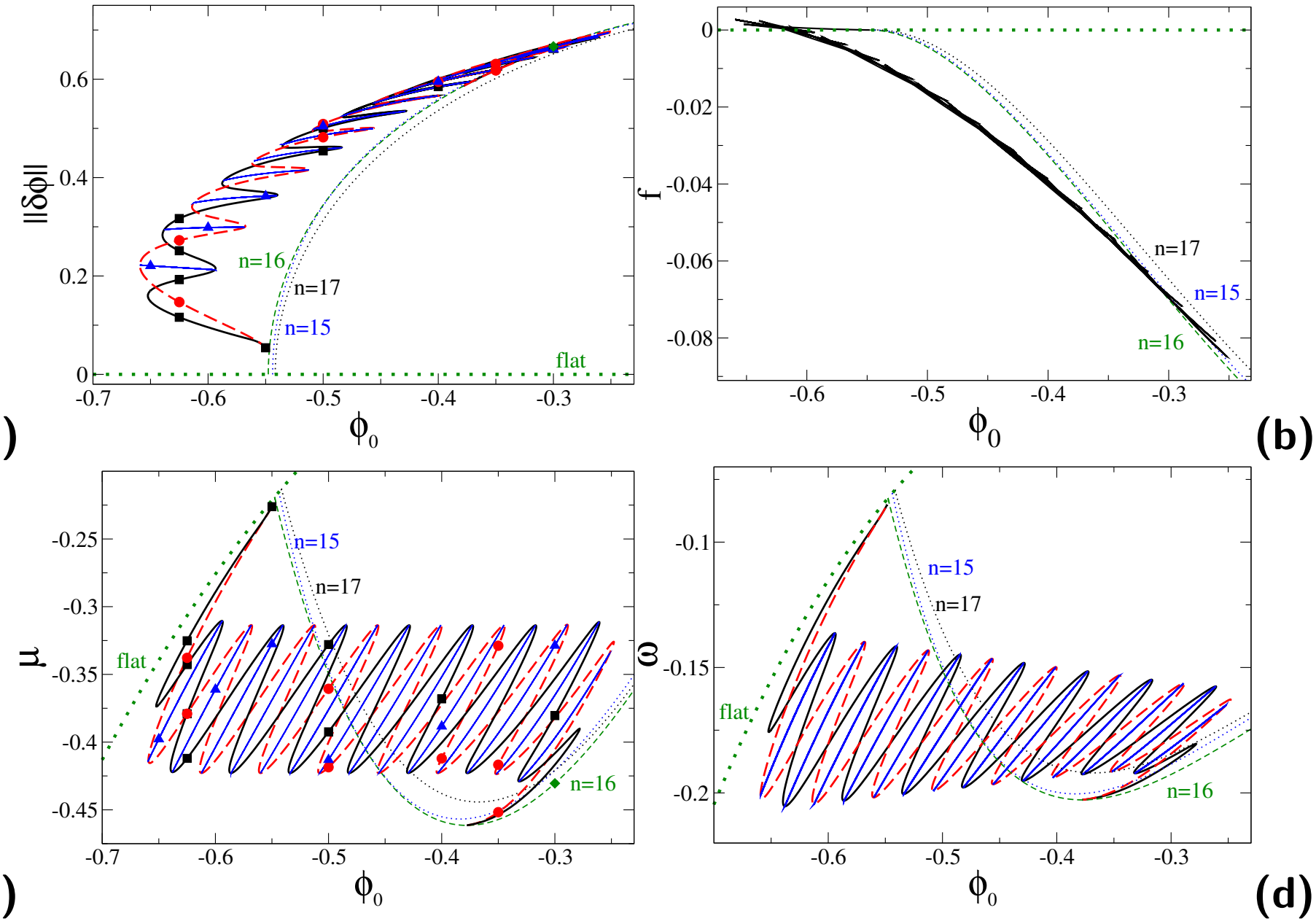

Bifurcation diagram for the 1D PFC model when $r = -0.9$, $L = 100$.

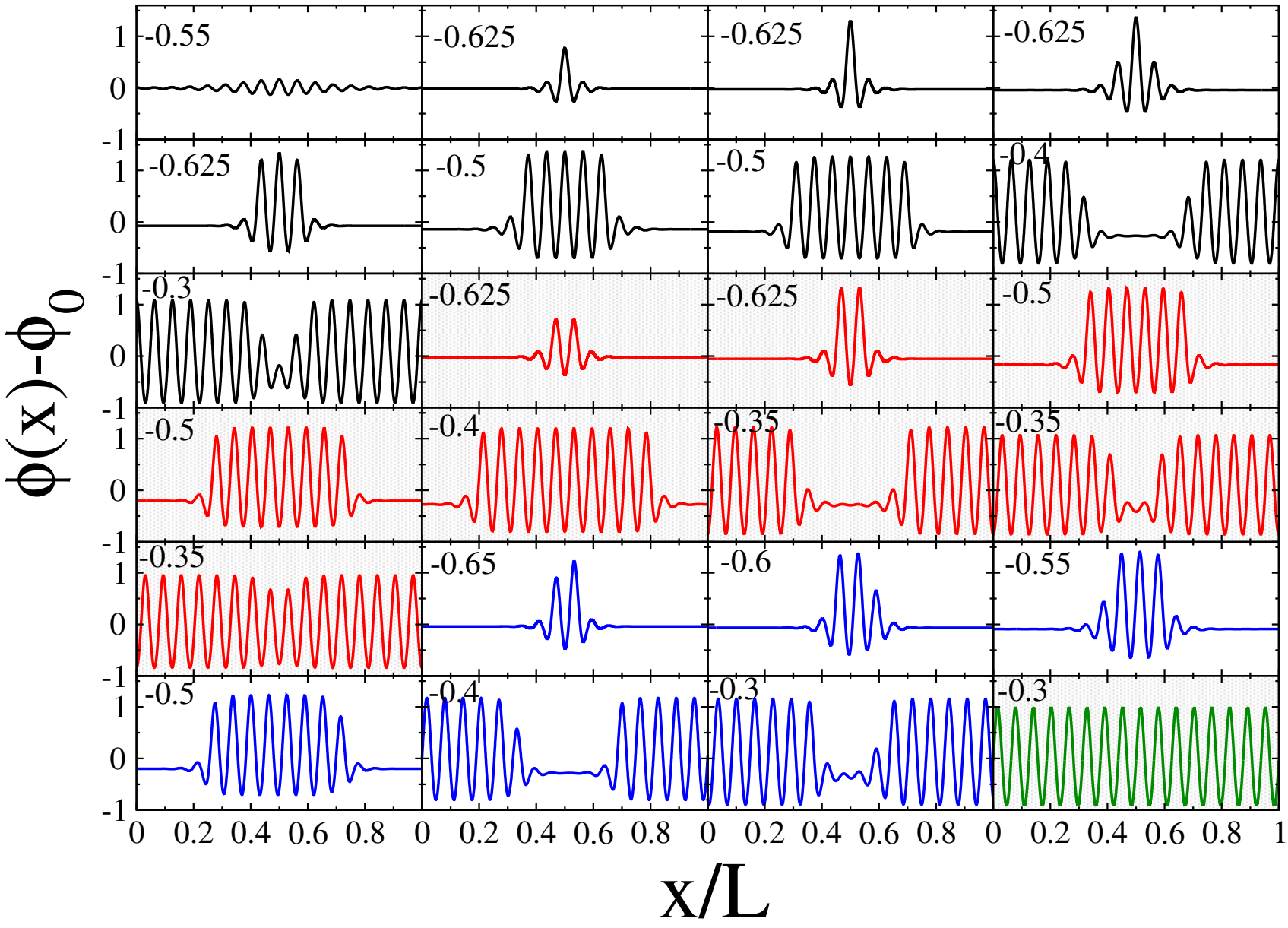
-0.55
-0.625
-0.625
-0.625
-0.625
-0.5
-0.5
-0.4
-0.3
-0.625
-0.625
-0.5
-0.5
-0.4
-0.35
-0.35
-0.35
-0.65
-0.6
-0.55
-0.5
-0.4
-0.3
-0.3
1
0
-1
0 0.2 0.4 0.6 0.8 1
φ(x)-φ0
x/L

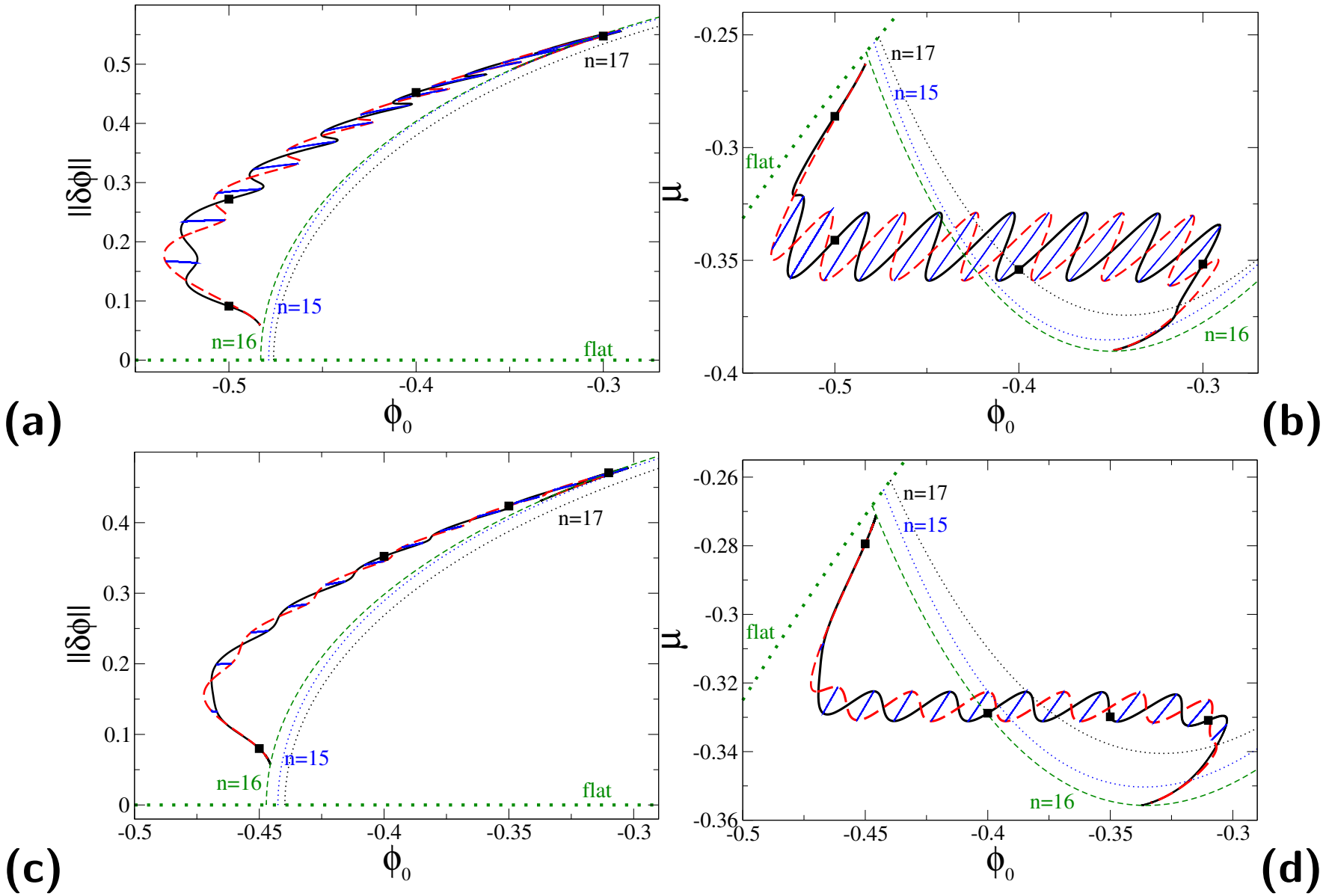

Bifurcation diagrams for (a,b) $r = -0.7$, (c,d) $r = -0.6$ and $L = 100$.

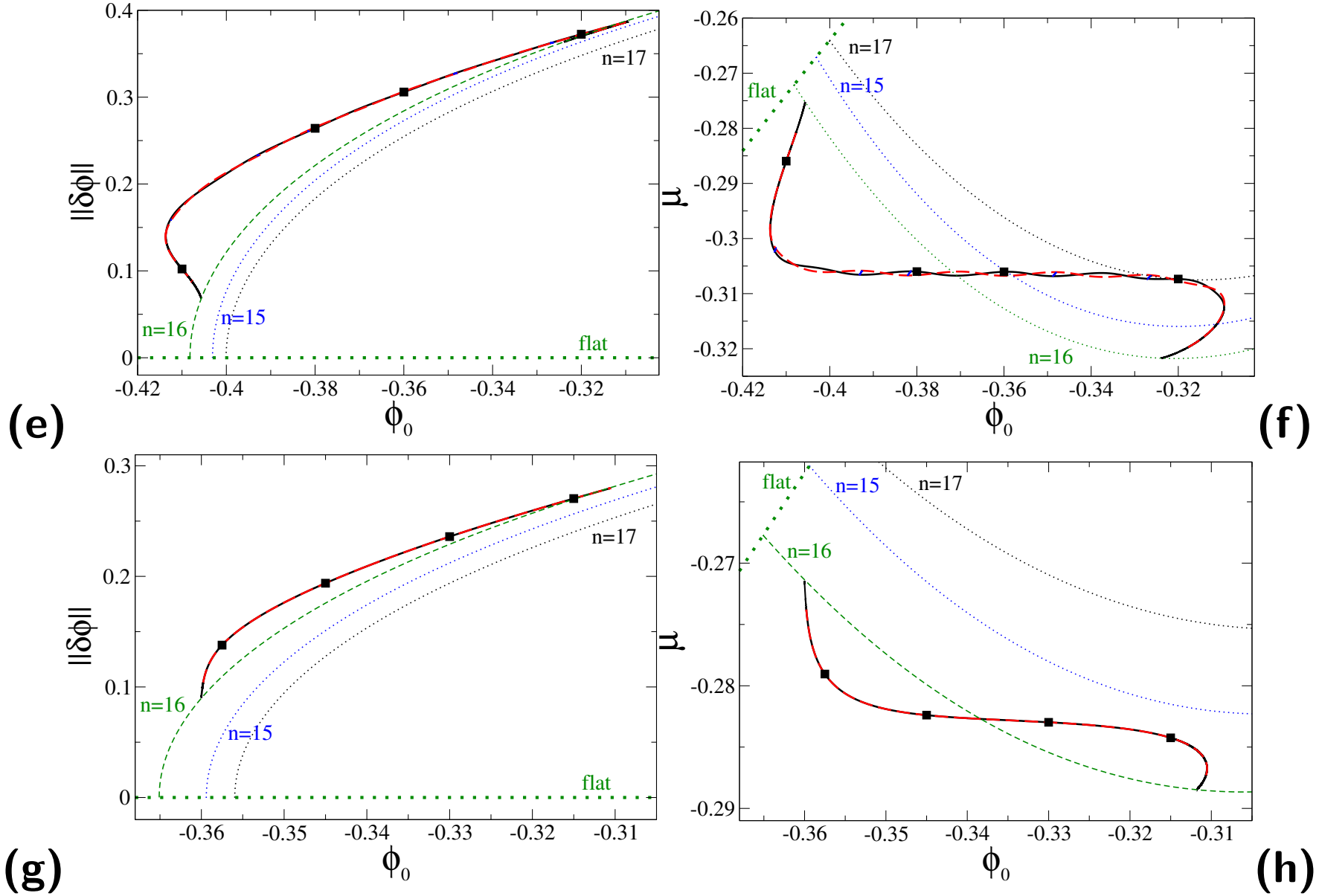

Bifurcation diagrams for (e,f) $r = -0.5$, (g,h) $r = -0.4$ and $L = 100$.

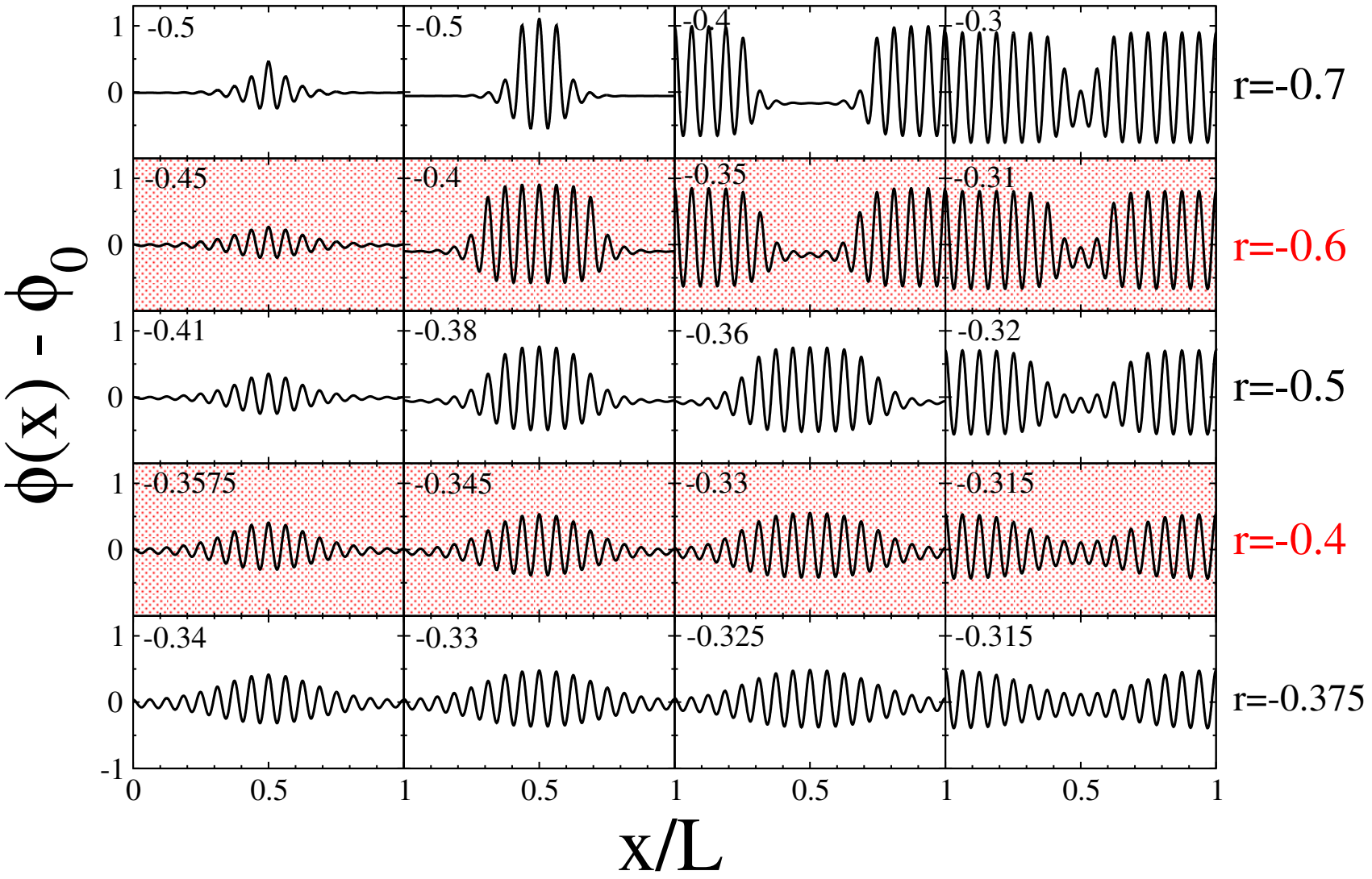

Solution profiles at different ϕ_0 values.

Stability

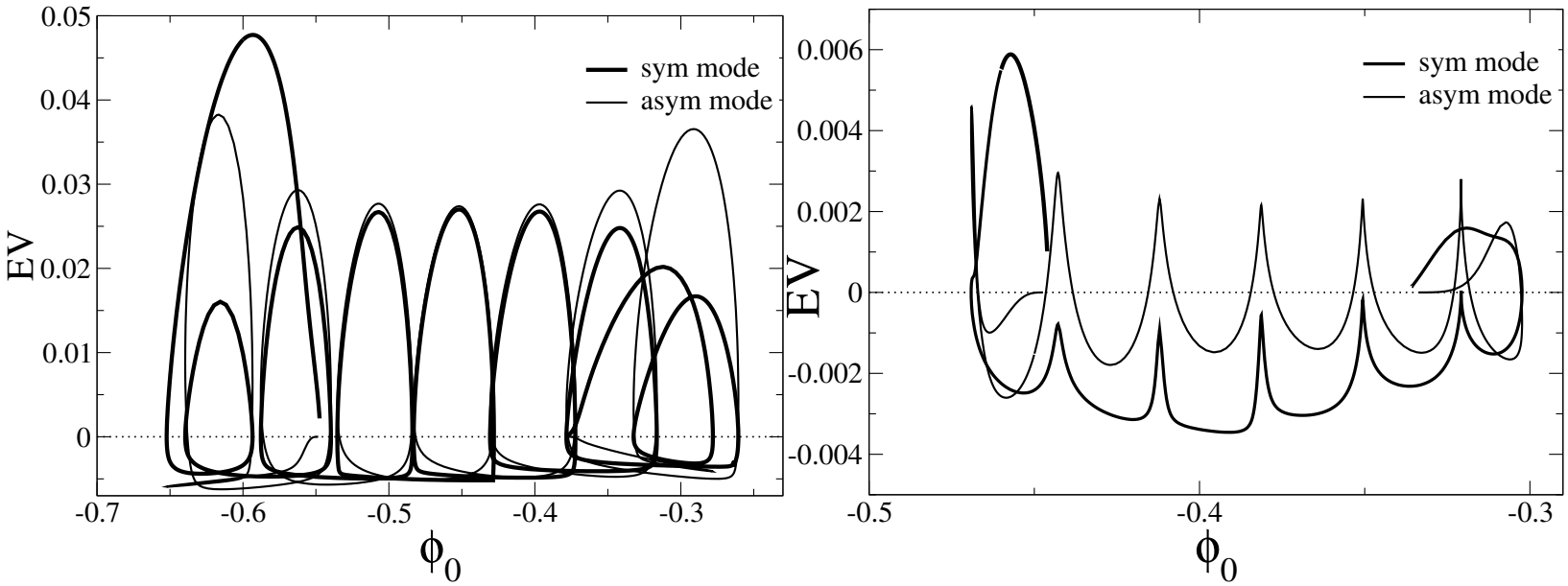

Leading eigenvalues of LS_{odd} for $r = -0.9$ and $r = -0.6$

Thiele et al., PRE **87**, 042915 (2013)

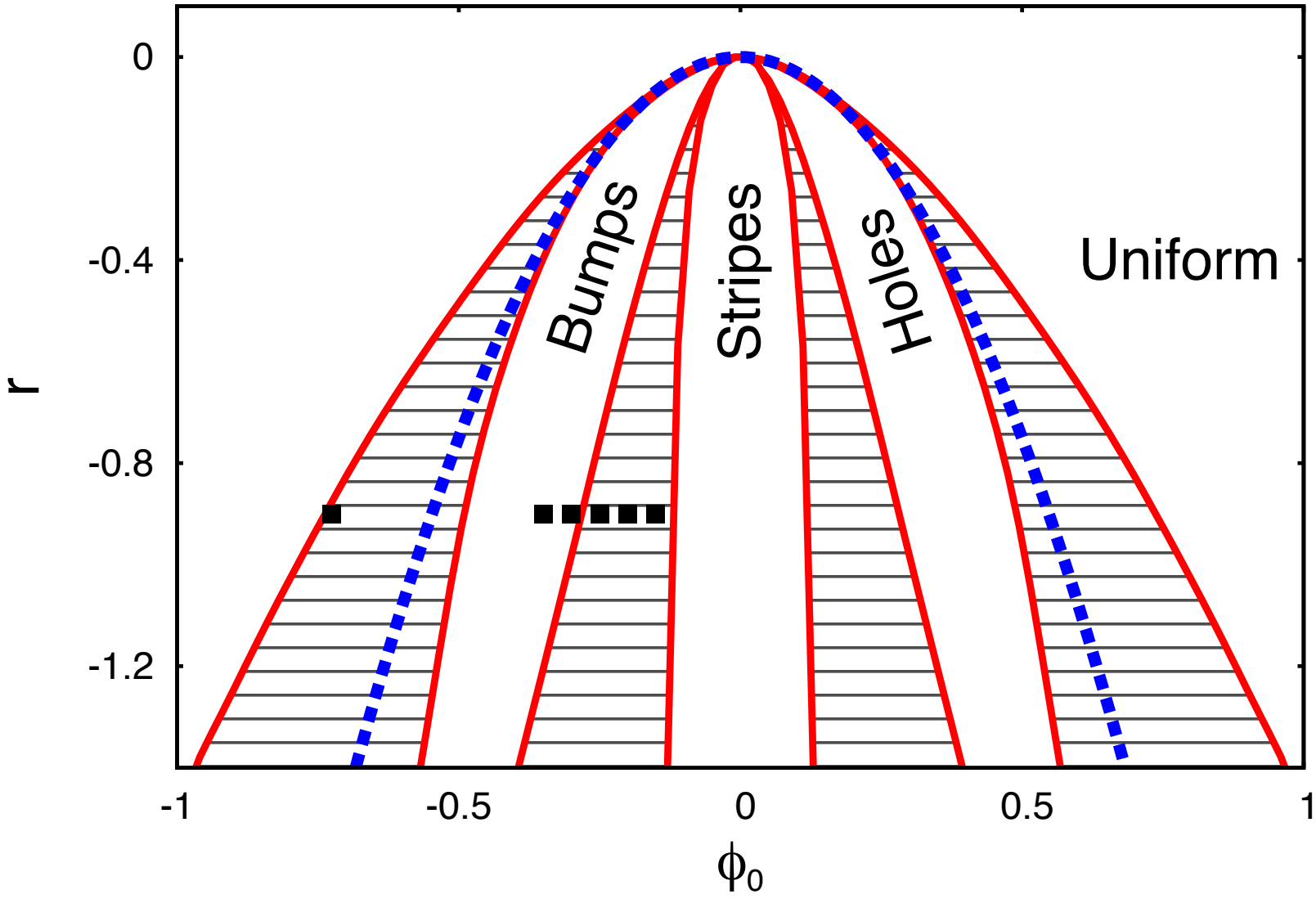

The phase diagram in 2D when $q = 1$

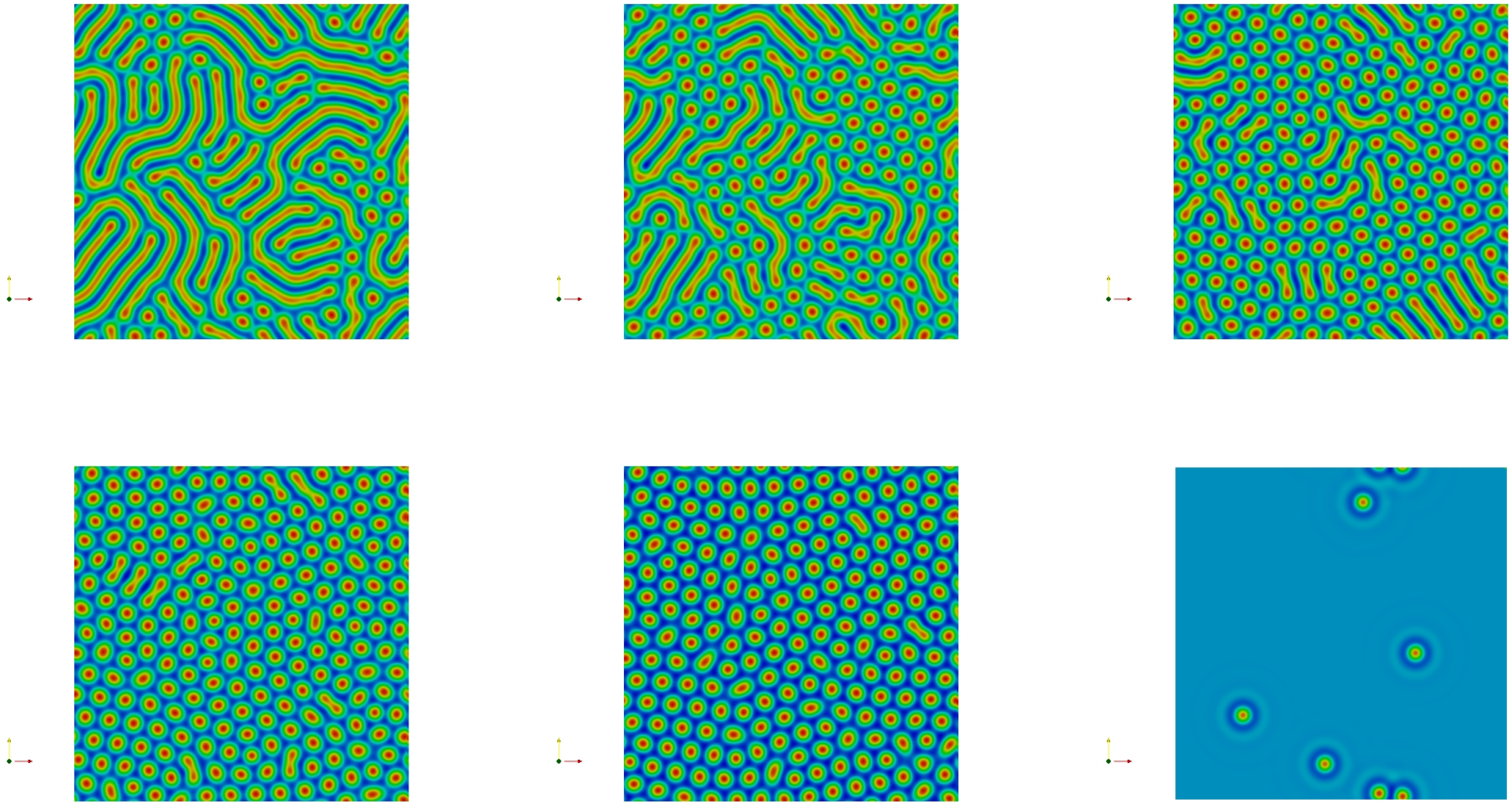

Solution profiles for $r = -0.9$ and $|\phi_0| = 0.15, 0.2, 0.25, 0.3, 0.35, 0.725$.

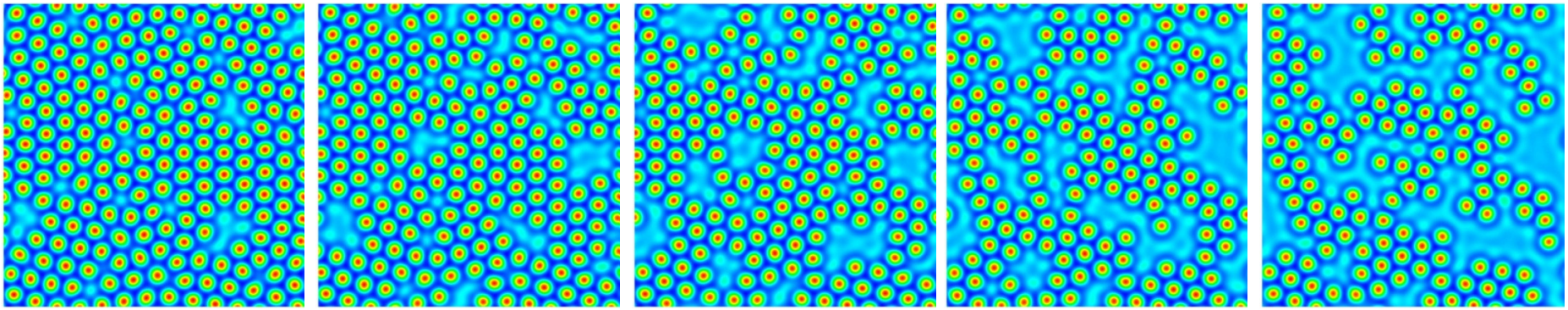

$\phi_0 = -0.450$ $\phi_0 = -0.475$ $\phi_0 = -0.500$ $\phi_0 = -0.525$ $\phi_0 = -0.550$

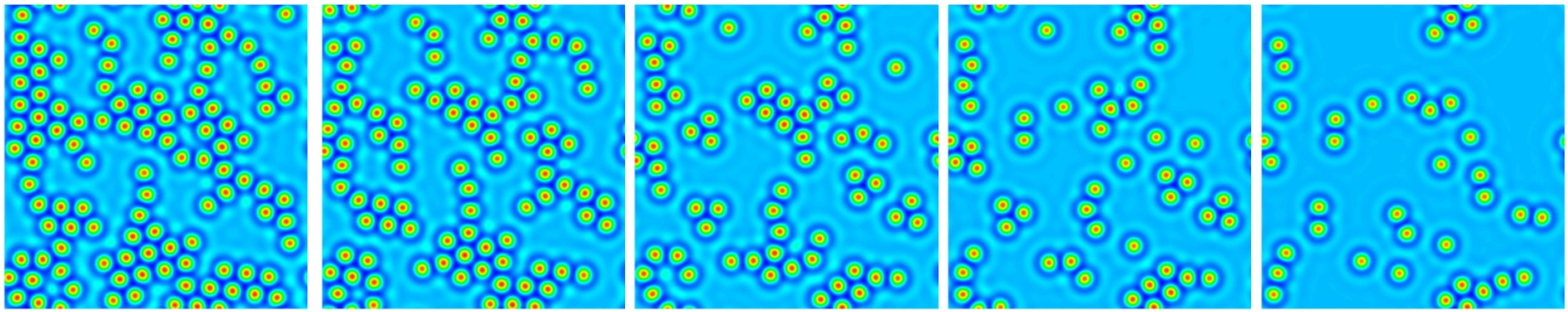

$\phi_0 = -0.575$ $\phi_0 = -0.600$ $\phi_0 = -0.625$ $\phi_0 = -0.650$ $\phi_0 = -0.675$

Thiele et al., PRE **87**, 042915 (2013)

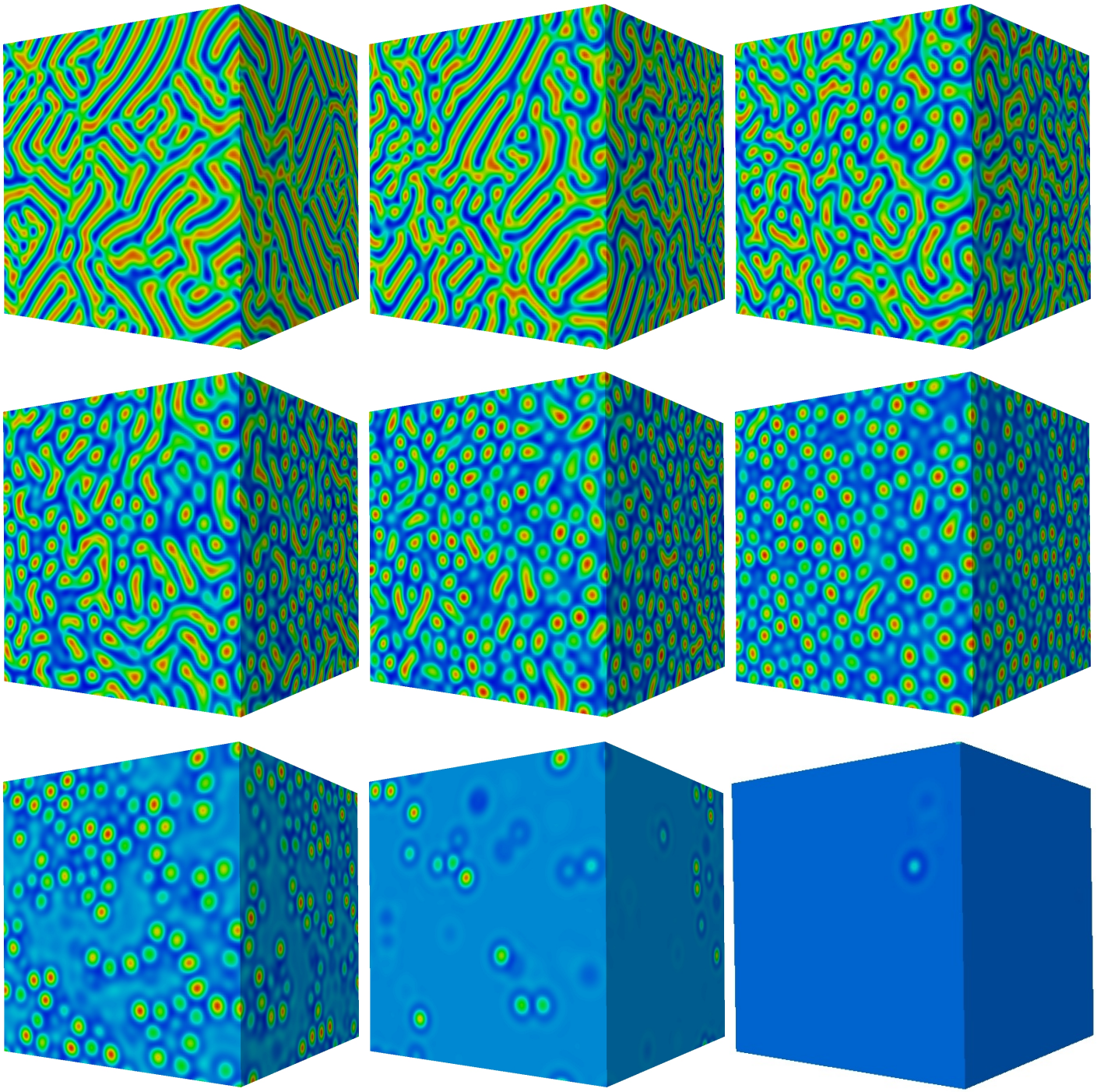

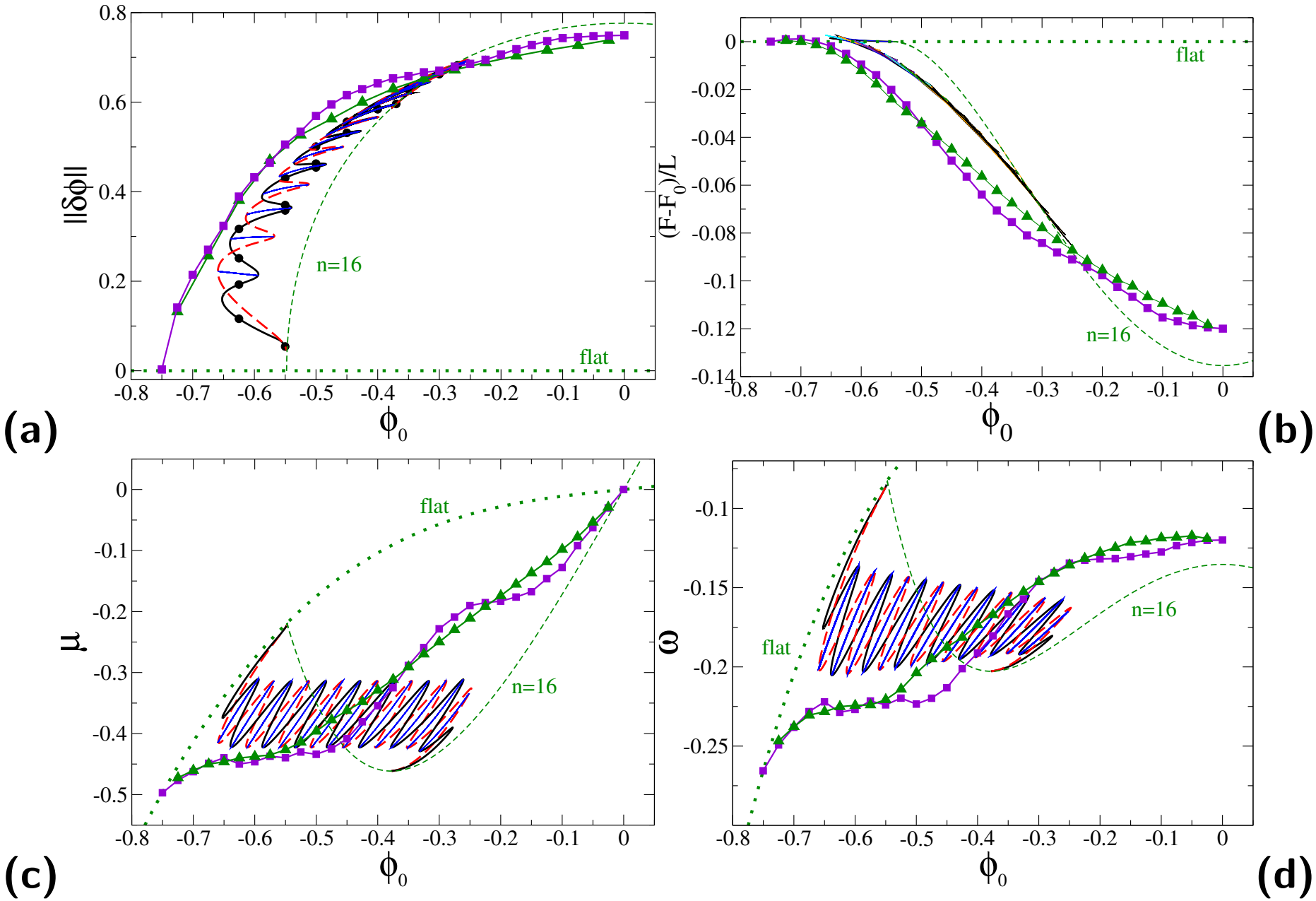

Superposition of the 2D and 3D results on top of the 1D results

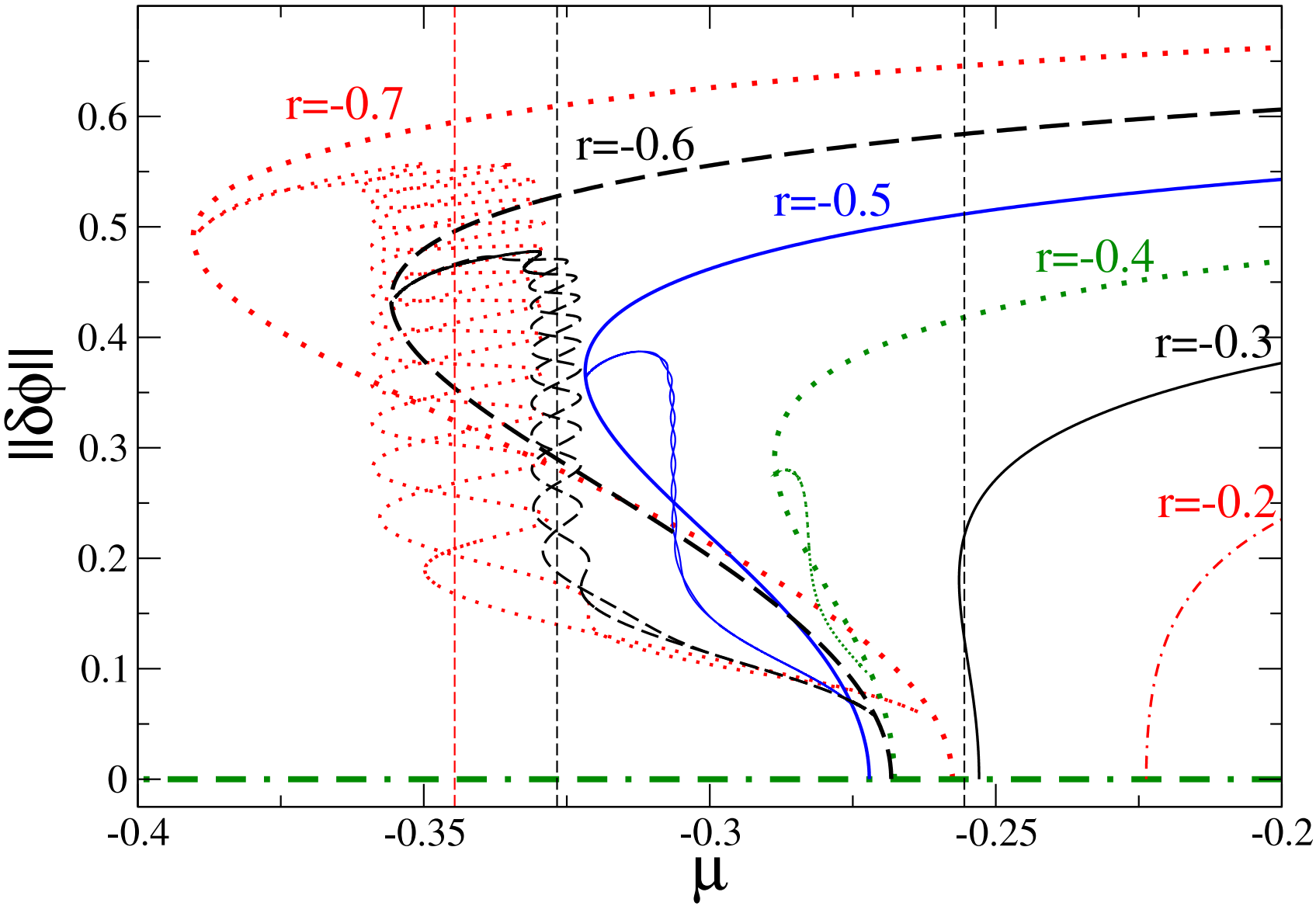

Slanted snaking plotted as a function of the chemical potential μ

The role of the longwave mode

We begin with the cSHE in the form

$$\phi_t = \alpha\partial_x^2[(r+q^4)\phi + \phi^3 + 2q^2\partial_x^2\phi + \partial_x^4\phi].$$

The linear problem for $\phi = \phi_0$ has solutions $\psi \propto \exp(\sigma t + ikx)$:

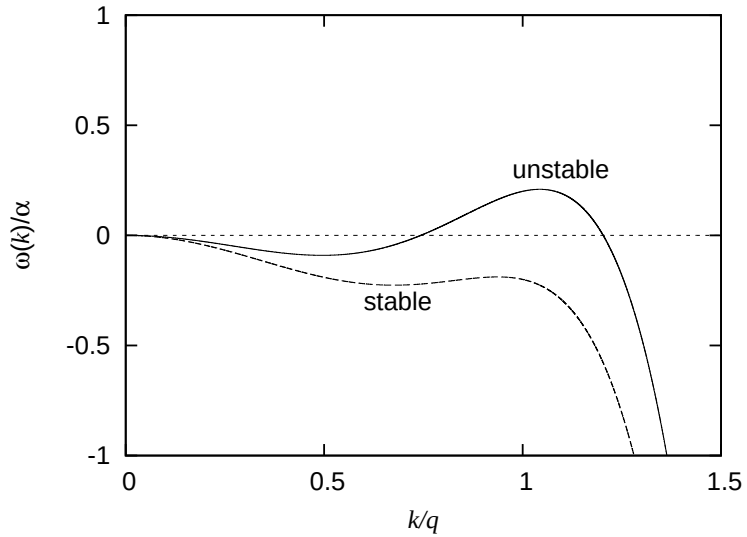

We therefore write $r = -3\phi_0^2 - \epsilon^2\nu$, where $\nu = \mathcal{O}(1)$ is positive and ϵ is a small parameter that defines how far r is from r_c. In this case a band of wavenumbers near $k = q$ grows slowly with growth rate $\sigma = \mathcal{O}(\epsilon^2)$, while wavenumbers near $k = 0$ decay at a similar rate. There is therefore time for these two disparate wavenumbers to interact.

The role of the longwave mode

These considerations suggest that we perform a two-scale analysis with a short scale $x = \mathcal{O}(q^{-1})$ and a long scale $X = \epsilon x$, so that $\partial_x \to \partial_x + \epsilon \partial_X$ etc. We also write

$$\psi = \epsilon A(X,t)e^{iqx} + \epsilon^2 B(X,t) + \epsilon^2 C(X,t)e^{2iqx} + \text{c.c.} + \mathcal{O}(\epsilon^3),$$

where the amplitudes A and C are complex and B is real. Substituting, we obtain

$$A_t = -\epsilon^2 \alpha q^2(-\nu A - 4q^2 A_{XX} + 6\phi_0 AB + 6\phi_0 CA^* + 3|A|^2 A) + \mathcal{O}(\epsilon^3),$$

$$B_t = \epsilon^2 \alpha(q^4 B_{XX} + 6\phi_0 |A|^2_{XX}) + \mathcal{O}(\epsilon^3),$$

and

$$C_t = -4\alpha q^2(9q^4 C + 3\phi_0 A^2) + \mathcal{O}(\epsilon).$$

Thus C evolves on an $\mathcal{O}(1)$ time scale to its asymptotic value, $C = -\phi_0 A^2/3q^4 + \mathcal{O}(\epsilon)$.

Weakly nonlinear theory

The remaining equations may be written in the form [Matthews and Cox, Nonlinearity **13**, 1293 (2000)]

$$A_t = \nu A + 4A_{XX} - \xi A\theta_X - 3\left(1 - \frac{\xi^2}{54}\right)|A|^2 A + \mathcal{O}(\epsilon),$$

$$\theta_t = \theta_{XX} + \xi|A|^2_X + \mathcal{O}(\epsilon)$$

where $B = \theta_X$. Here $\xi \equiv 6\phi_0/q^2 < 0$, and q has been absorbed into X and $\epsilon^2\alpha q^2$ into t. These equations describe the dynamics of the cSHE in the weakly nonlinear regime.

The coupling to the large scale mode θ requires $\xi \neq 0$ and destabilizes the primary supercritical branch of periodic states. The resulting spatially modulated states evolve into localized structures when this branch is followed to higher amplitude. Thus LS exist in the absence of bistability!

Solidification front at $r = -0.9$, $\phi_0 = -0.43$ ($\Delta = -0.35$)

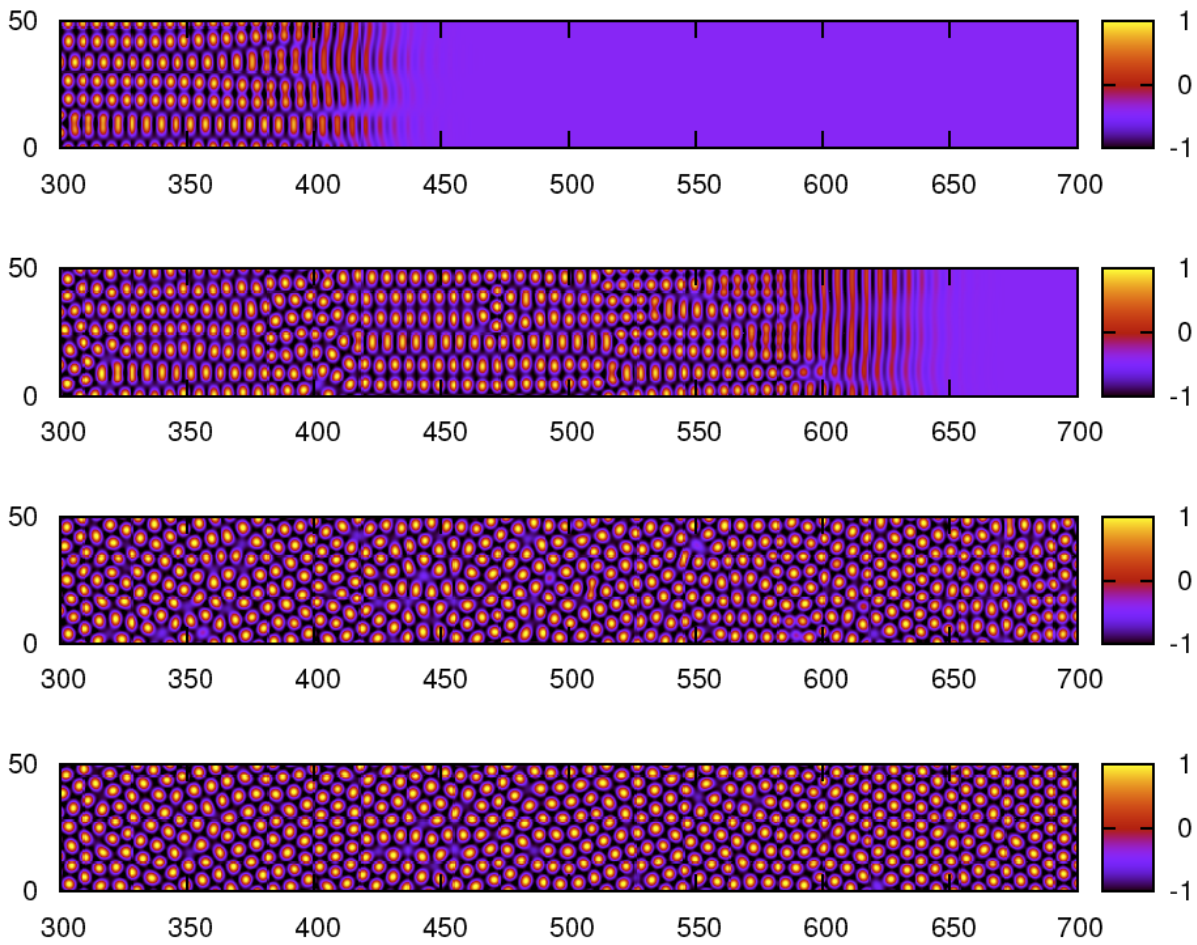

Archer et al., PRE **86**, 031603 (2012)

Solidification fronts: parameter dependence

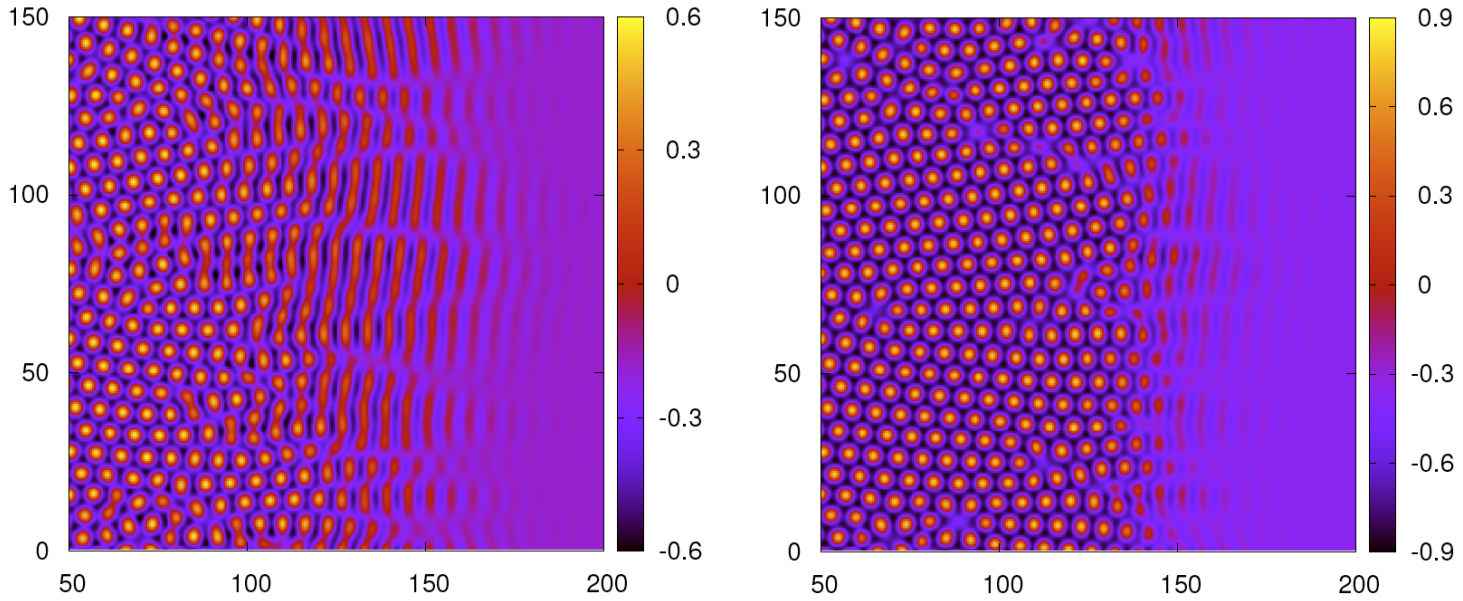

$r = -0.2,\ \phi_0 = -0.183$ $\qquad$ $r = -0.5,\ \phi_0 = -0.365$

Archer et al., PRE **86**, 031603 (2012)

Solidification fronts: parameter dependence

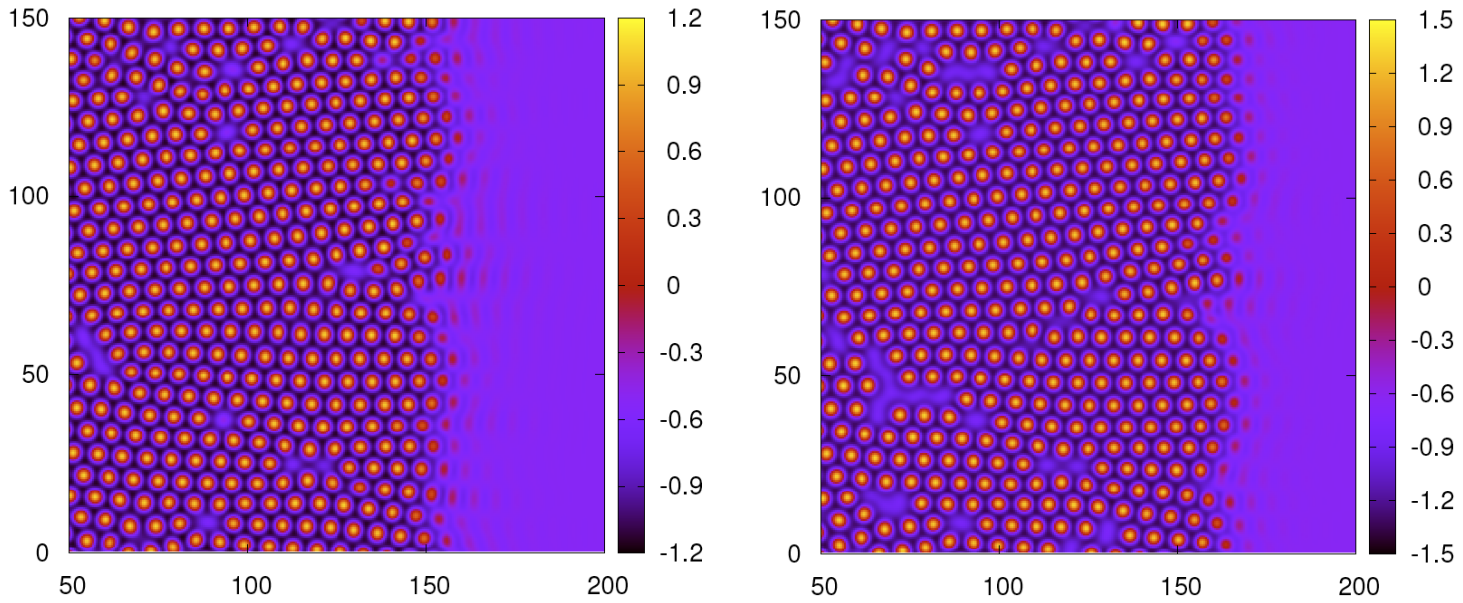

$r = -0.9,\ \phi_0 = -0.516$ $\qquad$ $r = -1.3,\ \phi_0 = -0.632$

Archer et al., PRE **86**, 031603 (2012)

Bond angle evolution for $r = -0.9$

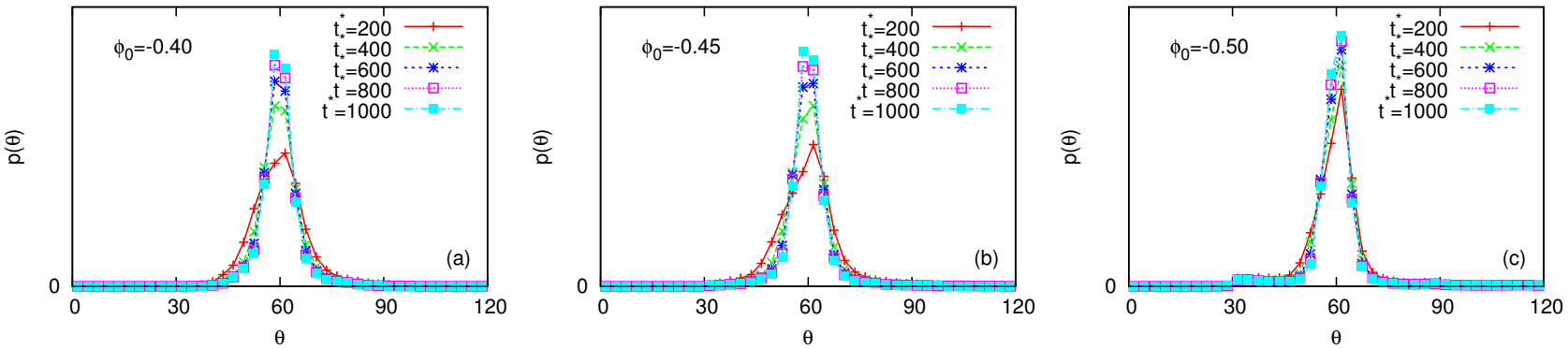

Archer et al., PRE **86**, 031603 (2012)

Radial correlation function for $r = -0.9$

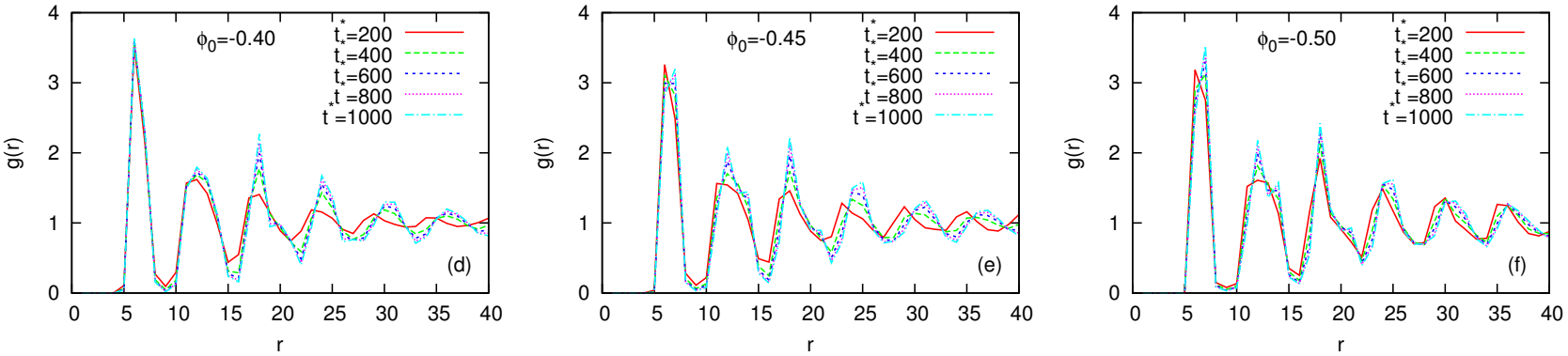

Archer et al., PRE **86**, 031603 (2012)

1D solidification front: $r = -0.9$, $\phi_0 = -0.4$

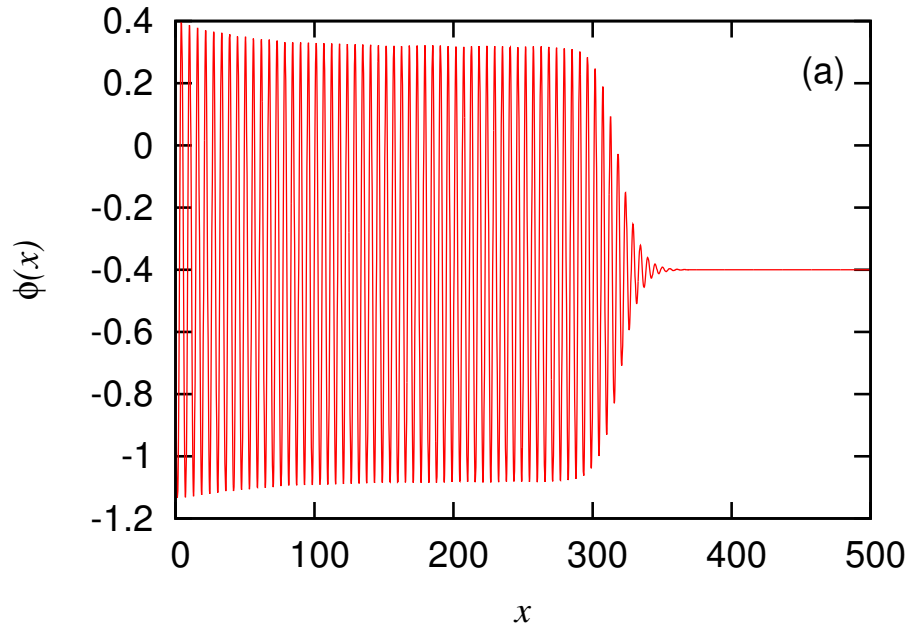

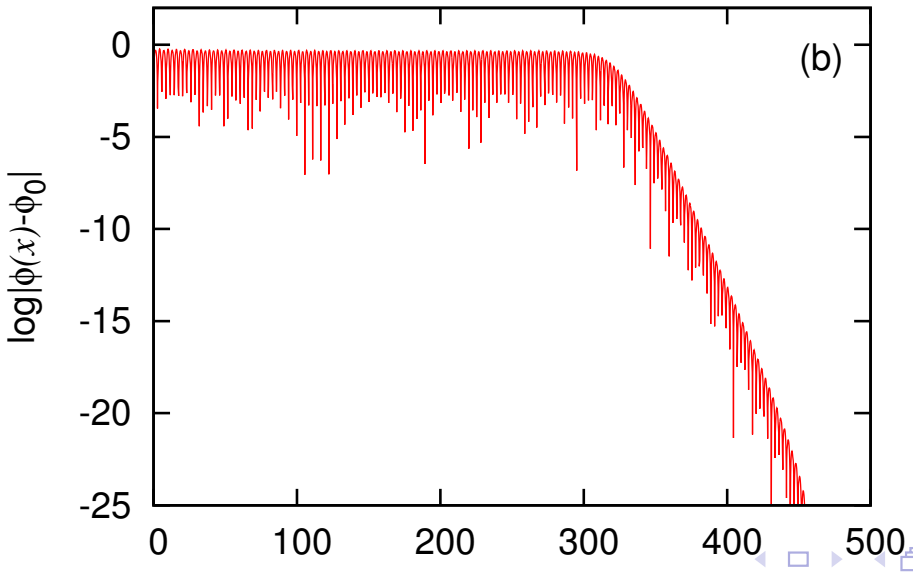

Speed of the solidification front

We assume that the speed of the front is determined by the marginal stability criterion of Dee and Langer, and write the linearized equation in the form

$$\sigma(k) = -\alpha k^2[\Delta + (q^2 - k^2)^2],$$

where $\Delta = r + 3\phi_0^2$. To determine the front speed we go into the reference frame of the front moving at speed c, $\Omega(k) = ick + \sigma(k)$, and solve

$$\frac{d\Omega}{dk} = 0 \qquad \mathrm{Re}(\Omega) = 0$$

for k_r, k_i and c as functions of Δ. The resulting density profile at the front is $\tilde{\rho}_{\mathrm{front}}(\xi, t) \sim \exp(-k_i\xi)\sin(k_r\xi + \mathrm{Im}(\Omega)t)$ relative to the front. The pattern left behind is period in space with wavenumner k^* given by conservation of nodes [Ben-Jacob et al, Physica D 14, 348 (1985)]

$$k^* = \frac{1}{c}\mathrm{Im}(\Omega) = k_r + \frac{1}{c}\mathrm{Im}[\sigma(k)].$$

Speed of the solidification front in 1D

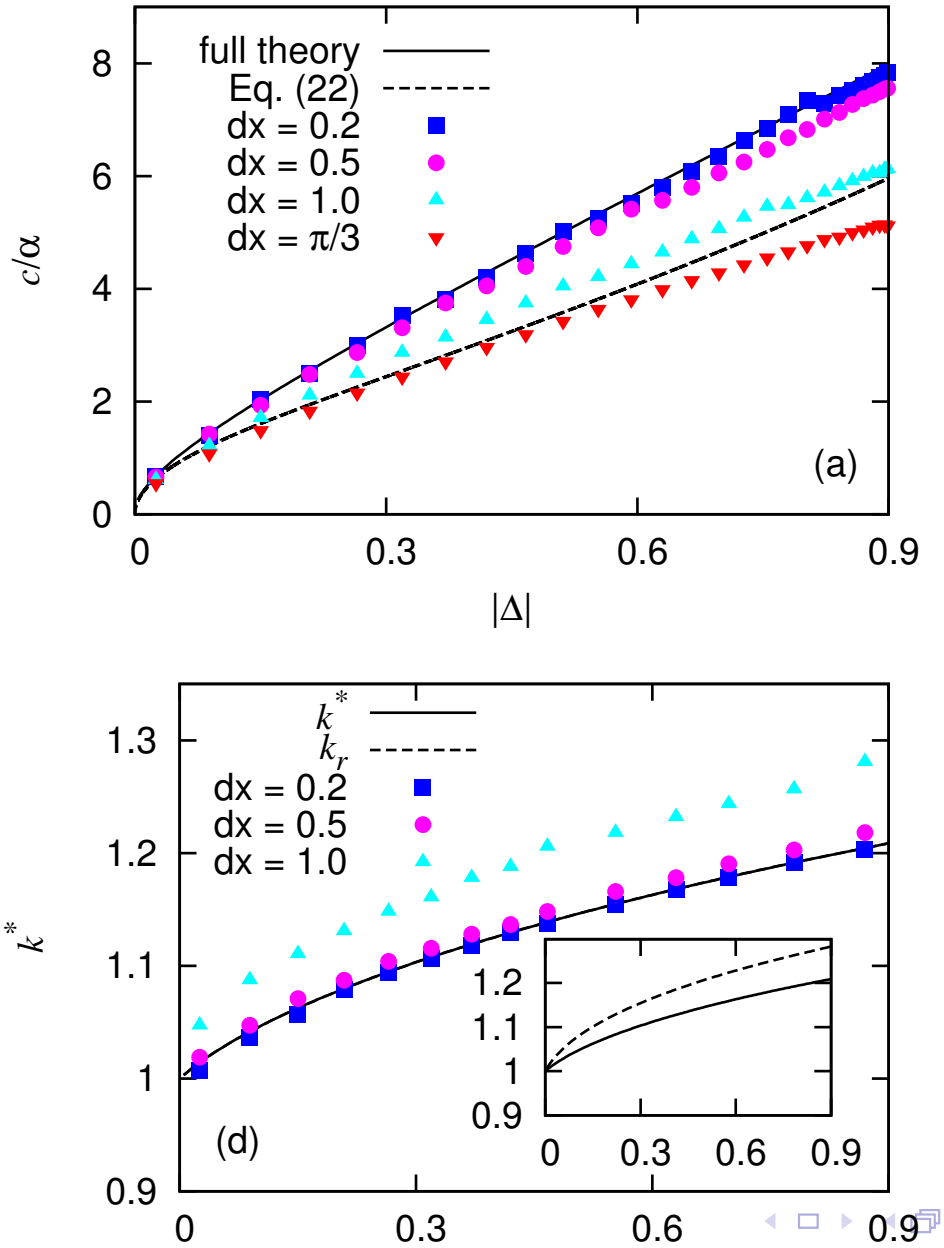

Speed of the solidification front in 1D

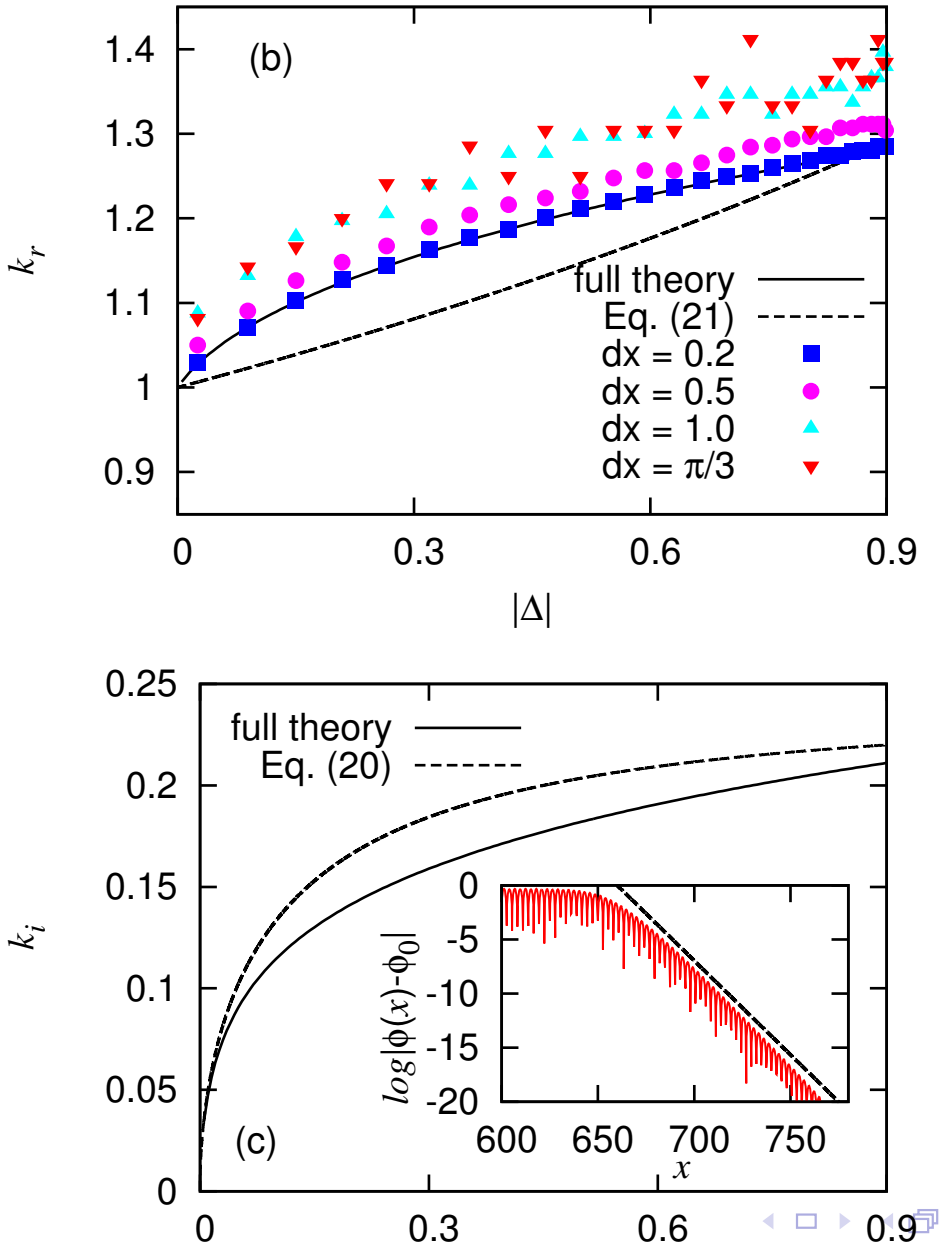

Speed of the solidification front in 2D

The 2D case is much complicated but also more interesting because of the competition between stripes (the first pattern to form) and hexagons (the final pattern to form):

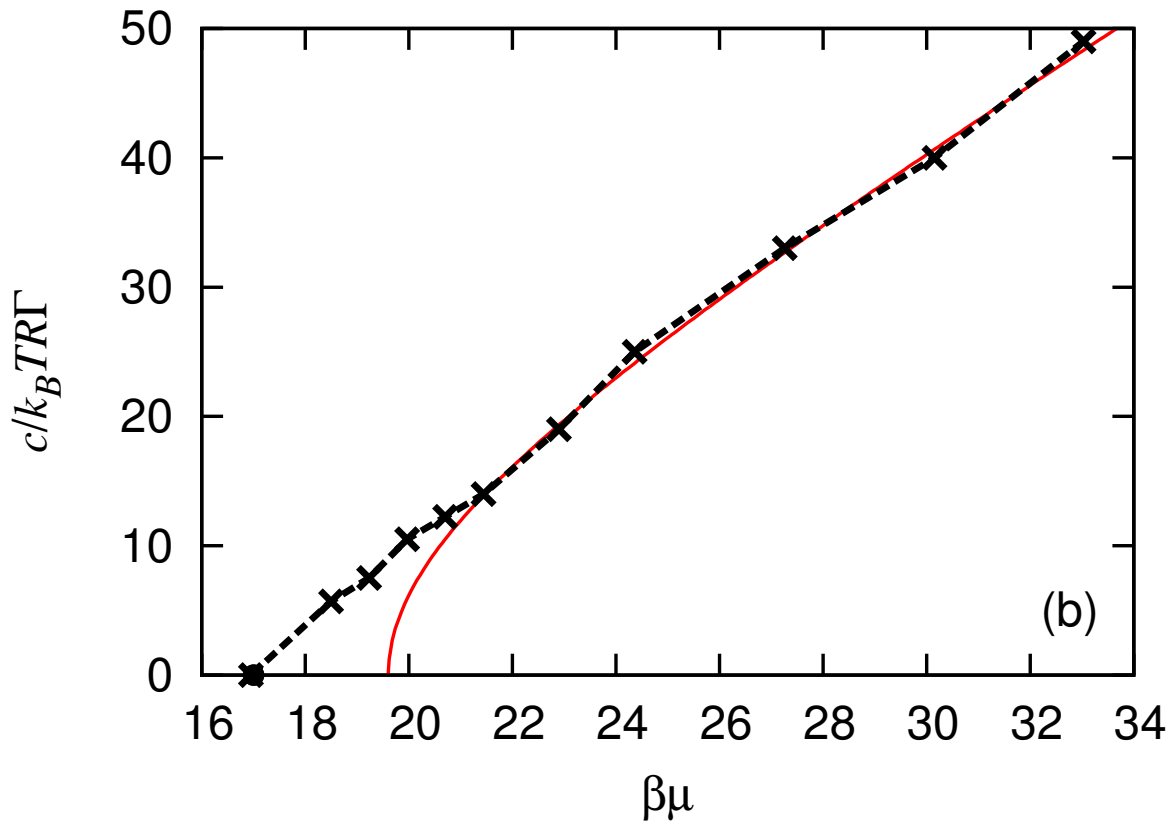

Fig. 1. The front velocity c as a function of the chemical potential μ from DNS of a GEM-4 fluid with temperature $k_B T/\epsilon = 1$ compared with the prediction of

Speed of the solidification front in 2D

Model equations:

$$\frac{\partial A_k}{\partial t} = \gamma A_k + \frac{\partial^2 A_k}{\partial x_k^2} + A^*_{[k-1]} A^*_{[k+1]} - (|A_k|^2 + \lambda |A_{[k-1]}|^2 + \lambda |A_{[k+1]}|^2),$$

where $k = 0, 1, 2$. Here A_k are the complex amplitudes of the three wavevectors $\mathbf{n}_0 \equiv (1, 0)k_c$, $\mathbf{n}_1 \equiv (-1, \sqrt{3})k_c/2$, $\mathbf{n}_2 \equiv (-1, -\sqrt{3})k_c/2$ in the (x, y) plane, and $x_k \equiv \mathbf{x} \cdot \mathbf{n}_k$ [Golubitsky et al., Physica D **10**, 249 (1984)]. Here k_c is the critical wave number at onset of the hexagon-forming instability ($\gamma = 0$), and $[k \pm 1] \equiv (k \pm 1)(\mathrm{mod} 3)$. These equations constitute a gradient flow with free energy

$$\mathcal{F} \equiv \int_{-\infty}^{\infty} \sum_{k=0}^{2} \left(\frac{1}{2} |\frac{\partial A_k}{\partial x_k}|^2 - V \right) dx,$$

where

$$V \equiv \sum_{k=0}^{2} \left(\frac{1}{2}\gamma |A_k|^2 - \frac{1}{4}|A_k|^4 \right) - \frac{\lambda}{2}(|A_0|^2|A_1|^2 + |A_1|^2|A_2|^2 + |A_2|^2|A_0|^2) + A_0^* A_1^* A_2^*.$$

Speed of the solidification front in 2D

We focus on planar fronts perpendicular to $\mathbf{n}_0 \equiv (1,0)k_c$ and thus focus on solutions independent of the variable y along the front. Symmetry with respect to $y \to -y$ implies the presence of solutions with $A_1 = A_2 \equiv B$, say. Absorbing the wave number k_c in the variable x, and writing $A_0 \equiv A$ we obtain the equations

$$\frac{\partial A}{\partial t} = \frac{\partial^2 A}{\partial x^2} + \gamma A + B^2 - A^3 - 2\lambda A B^2$$

$$\frac{\partial B}{\partial t} = \frac{1}{4}\frac{\partial^2 B}{\partial x^2} + \gamma B + AB - (1+\lambda)B^3 - \lambda A^2 B.$$

In writing these equations we have assumed that A and B are real in order to focus on the behavior of the amplitudes, thereby setting the phase $\Phi \equiv \arg(A) + 2\arg(B) = 0$. This phase distinguishes so-called up-hexagons from down-hexagons [Golubitsky et al., Physica D **10**, 249 (1984)].

Speed of the solidification front in 2D

These equations have solutions in the form of regular hexagons $(A, B) = (A_h, A_h)$, stripes $(A, B) = (A_r, 0)$ and the homogeneous liquid state $(A, B) = (0, 0)$, where

$$A_h = \frac{1 + \sqrt{1 + 4\gamma(1 + 2\lambda)}}{2(1 + 2\lambda)}, \qquad A_r = \sqrt{\gamma},$$

and are critical points of the potential $V(A, B) = \frac{1}{2}\gamma(A^2 + 2B^2) + AB^2 - [\frac{1}{4}A^4 + \lambda A^2 B + \frac{1}{2}(1 + \lambda)B^4]$. Note that without loss of generality we have taken $A_h > 0$, $A_r > 0$ since negative values can be compensated for by choosing $\Phi = \pi$, i.e., by an appropriate spatial translation.
The hexagons and the liquid state coexist stably in the subcritical regime, $-[4(1 + 2\lambda)]^{-1} < \gamma < 0$; the liquid state becomes unstable when $\gamma > 0$. A front traveling with speed c to the right, connecting the hexagonal state on the left with the liquid state to the right, takes the form

$$A(x, t) = \tilde{A}(\xi), \quad B(x, t) = \tilde{B}(\xi), \quad \xi \equiv x - ct.$$

Speed of the solidification front in 2D

Thus

$$\frac{\partial^2 \tilde{A}}{\partial \xi^2} + c\frac{\partial \tilde{A}}{\partial \xi} + \gamma \tilde{A} + \tilde{B}^2 - \tilde{A}^3 - 2\lambda \tilde{A}\tilde{B}^2 = 0,$$

$$\frac{1}{4}\frac{\partial^2 \tilde{B}}{\partial \xi^2} + c\frac{\partial \tilde{B}}{\partial \xi} + \gamma \tilde{B} + \tilde{A}\tilde{B} - (1+\lambda)\tilde{B}^3 - \lambda \tilde{A}^2 \tilde{B} = 0$$

with the boundary conditions

$$\tilde{A} = \tilde{B} = A_h \quad \text{as} \quad \xi \to -\infty, \qquad \tilde{A} = \tilde{B} = 0 \quad \text{as} \quad \xi \to \infty.$$

The speed c vanishes in the subcritical regime when $\gamma = \gamma_0 < 0$ defined by the requirement $V(A_h, A_h) = V(0,0) = 0$ and is positive for $\gamma > \gamma_0$ ($V(A_h, A_h) < 0$) and negative for $\gamma < \gamma_0$ ($V(A_h, A_h) > 0$). An elemetary calculation gives $\gamma_0 = -2[9(1+2\lambda)]^{-1}$. The situation is more complicated in the supercritical regime where $\gamma > 0$ because this regime contains supercritical (but unstable!) stripes oriented parallel to the front. As a result one now finds fronts that connect the hexagonal structure to the stripe pattern and the stripe pattern to the liquid state, in addition to the front connecting the hexagonal structure and the (unstable) liquid state.

Speed of the solidification front in 2D

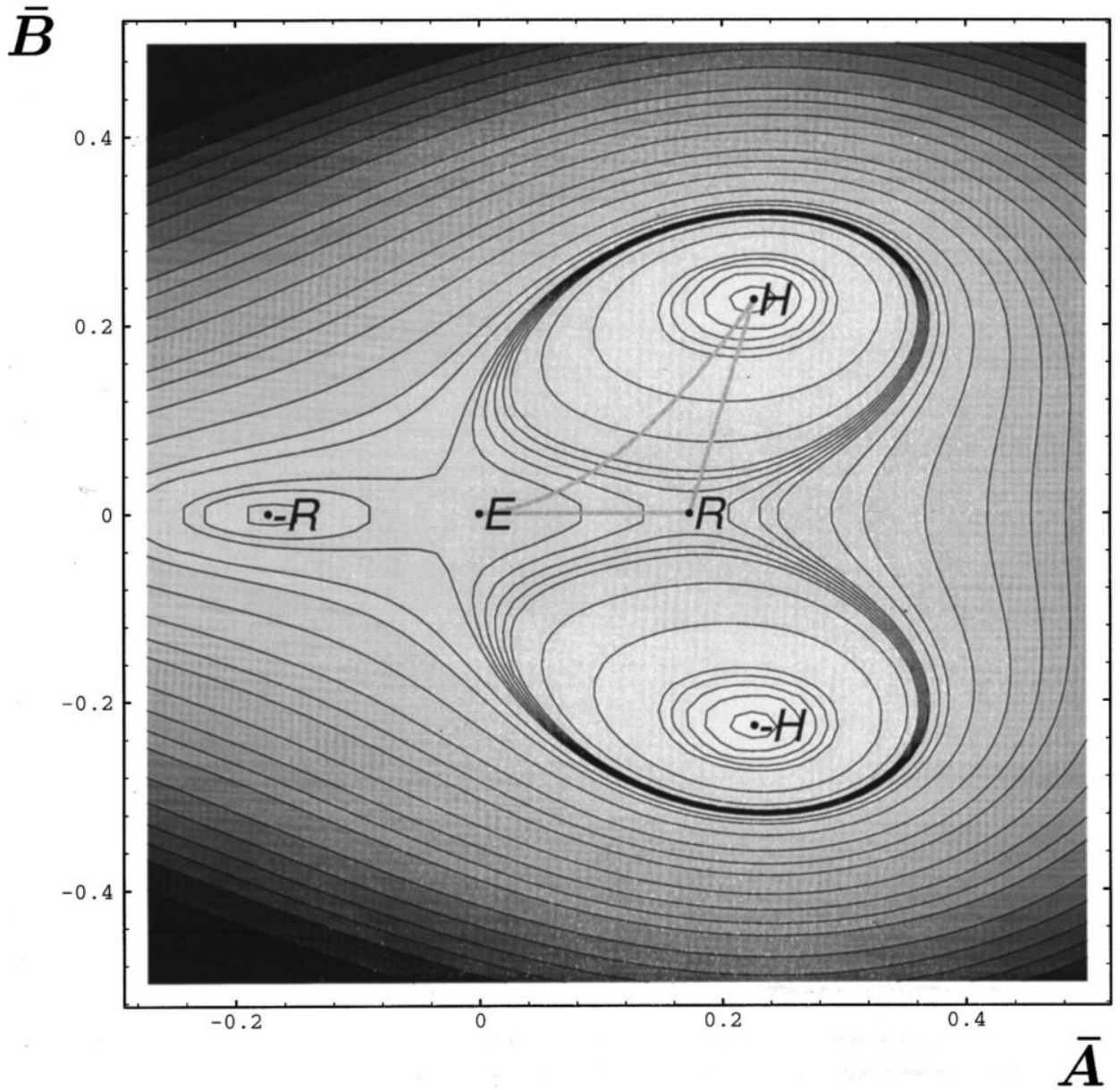

Speed of the solidification front in 2D

The marginal stability condition implies that stripes invade the homogeneous state with speed $c_e = 2\sqrt{\gamma}$, while an analogous calculation shows that the hexagons invade the unstable stripes with speed $c_r = [\sqrt{\gamma} - (\lambda - 1)\gamma]^{1/2}$ (Hari & Nepomnyashchyy, PRE **61**, 4835 (2000)). This speed exceeds c_e in the interval $0 < \gamma < (\lambda + 3)^{-2}$.
It is evident that the speed c_e cannot be selected when γ is too close to threshold since c remains positive for all $\gamma > \gamma_0$. In the spatial dynamics picture of the front one seeks a heteroclinic connection between $(\tilde{A}, \tilde{A}) = (A_h, A_h)$ and $(0, 0)$. Near $(0, 0)$ we have the asymptotic behavior

$$\tilde{A} \sim e^{\kappa_A \xi} \qquad \tilde{B} \sim e^{\kappa_B \xi}, \qquad \text{as} \quad \xi \to \infty,$$

where

$$\kappa_A^{\pm} = -\frac{c}{2} \pm \frac{1}{2}\sqrt{c^2 - 4\gamma}, \quad \kappa_B^{\pm} = -2c \pm 2\sqrt{c^2 - \gamma}.$$

Evidently, for $\gamma < 0$ the stable manifold of $(0, 0)$ is two-dimensional, and since one expects the heteroclinic to connect to $(0, 0)$ along the slow direction one anticipates that the solution will approach $(0, 0)$ in the "A" direction, with $\tilde{A} \sim e^{\kappa_A^- \xi}$ as $\xi \to \infty$.

Speed of the solidification front in 2D

However, as soon as $\gamma > 0$ the stable manifold of $(0,0)$ becomes four-dimensional, and the slowest direction is suddenly $\tilde{A} \sim e^{\kappa_A^+ \xi}$. H&N solve the problem numerically and find that for $c < 2\sqrt{\gamma}$ the front speed departs from the prediction $c = c_e$ and instead follows a speed $c = c_0$ for which the asymptotic behavior of the front continues to be $\tilde{A} \sim e^{\kappa_A^- \xi}$ as $\xi \to \infty$, thereby providing a smooth connection to the speed computed for $\gamma < 0$. We refer to the value of γ at which $c_h = c_e$ as $\gamma = \gamma_1$. H&N also show that in the region $\gamma_1 < \gamma < \gamma_2 \equiv (\lambda + 3)^{-2}$ both the front connecting the hexagonal state to the stripes and the front connecting the stripes to the liquid state travel with the same speed c_e. As a result the width of the stripe region between the hexagons and the liquid state remains constant; in numerical simulations this width is independent of the initial conditions, despite the nonuniqueness of the overall front solution, and to increase with γ. Finally, for $\gamma > \gamma_2$ the front speed $c_e > c_r$ and the front connecting the stripes to the liquid state outruns the hexagons invading the stripes and the width of the stripe interval in front of the hexagons grows without bound.

Speed of a solidification front in 2D: model problem

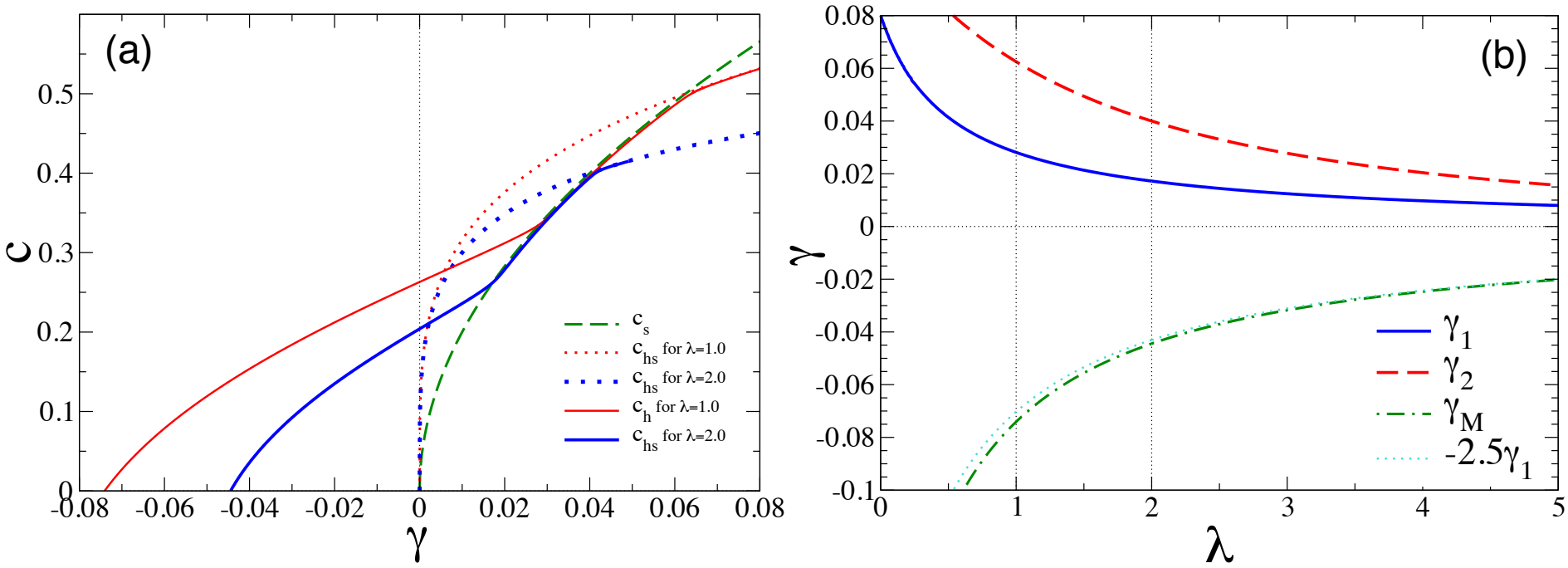

We define $\gamma = \gamma_1$ as the point of intersection of c_h and c_s and $\gamma = \gamma_2$ as the point $c_{hs} = c_s$. The model predicts that $\gamma_M \approx -2.5\gamma_1$ for all λ, a result that is not in agreement with the GEM-8 simulation.

Two-component system: equilibrium state in GEM-8

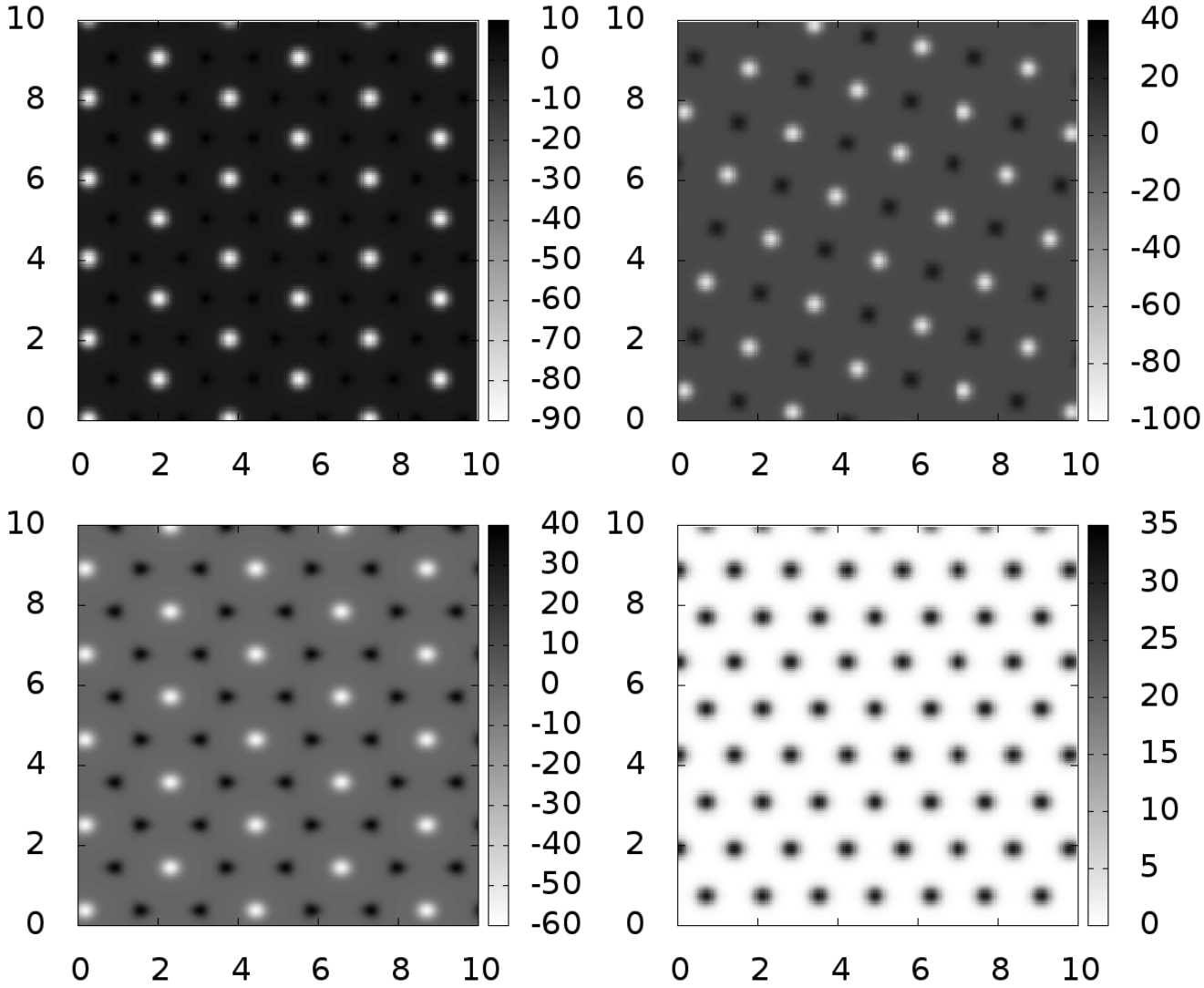

Equilibrium structures for density $\rho R_{11}^2 = 4$ and for $\rho_1/\rho = 0.1$, 0.25, 0.5 and 0.9 from left to right, with $\rho = \rho_1 + \rho_2$, $\epsilon_{ij} = \epsilon = k_B T$, $R_{22}/R_{11} = 1.5$, $R_{12}/R_{11} = 1$.

Two-component system: front propagation in 2D

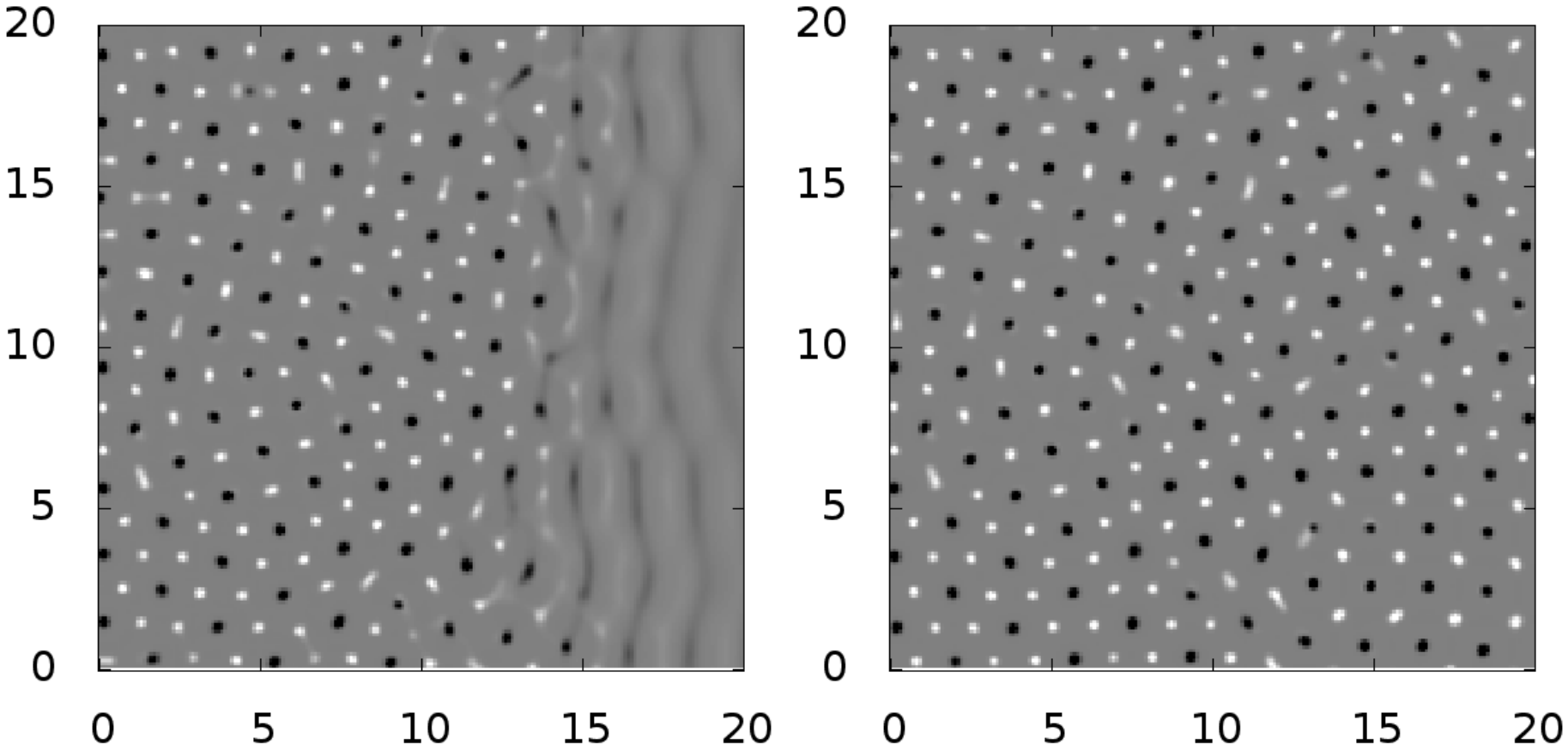

Snapshots from an advancing solidification front from the GEM-8 mixture advancing into an unstable fluid with $(\rho_1 + \rho_2)R^2 = 8$ and $\rho_1/(\rho_1 + \rho_2) = 0.5$, $\epsilon_{ij} = \epsilon = k_B T$ for $i, j = 1, 2$ and $R_{22} = R_{11} = R$.

Two-component system: $t = 2$ (top), $t = 400$ (bottom)

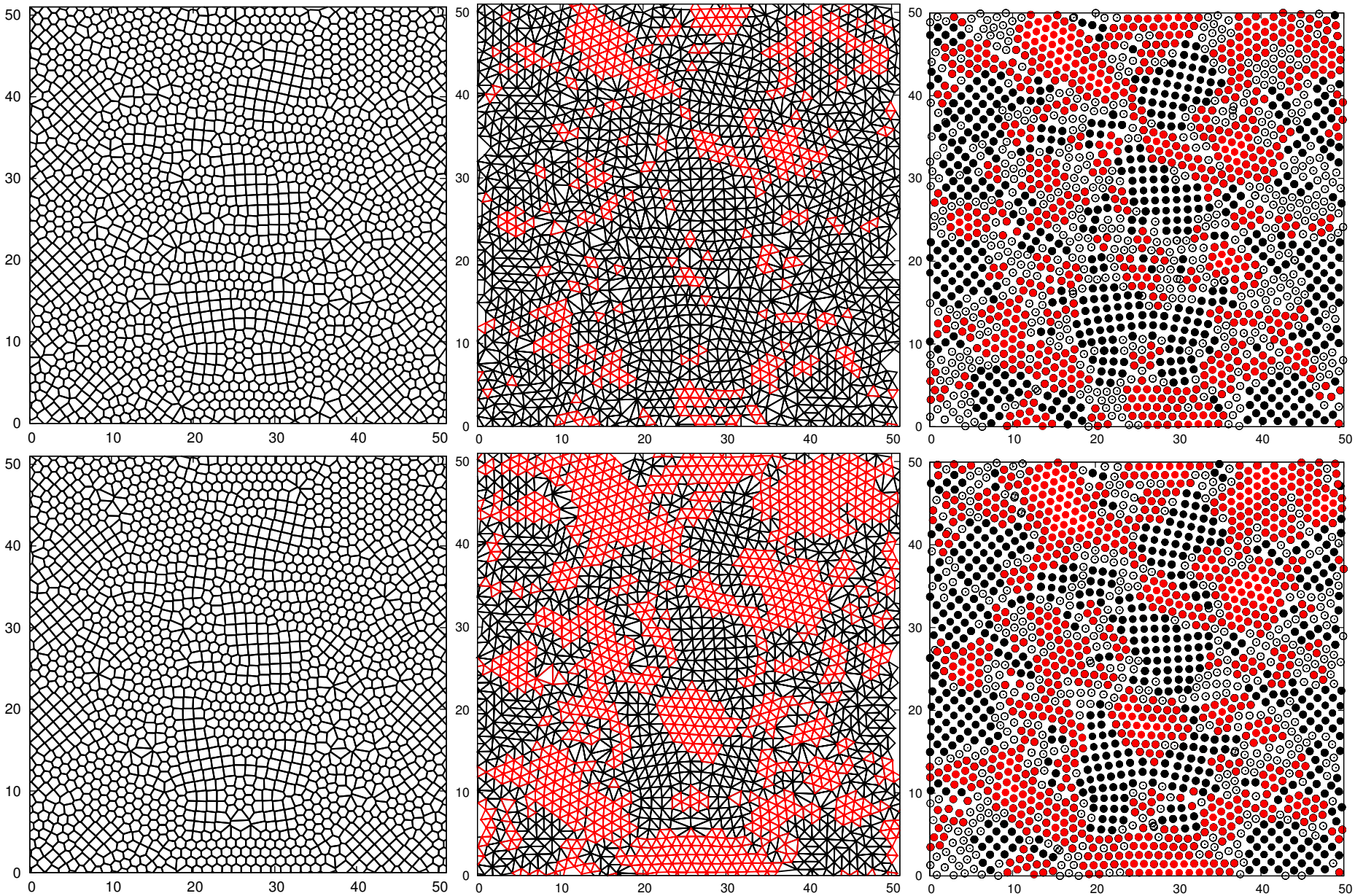

Two-component system: ageing

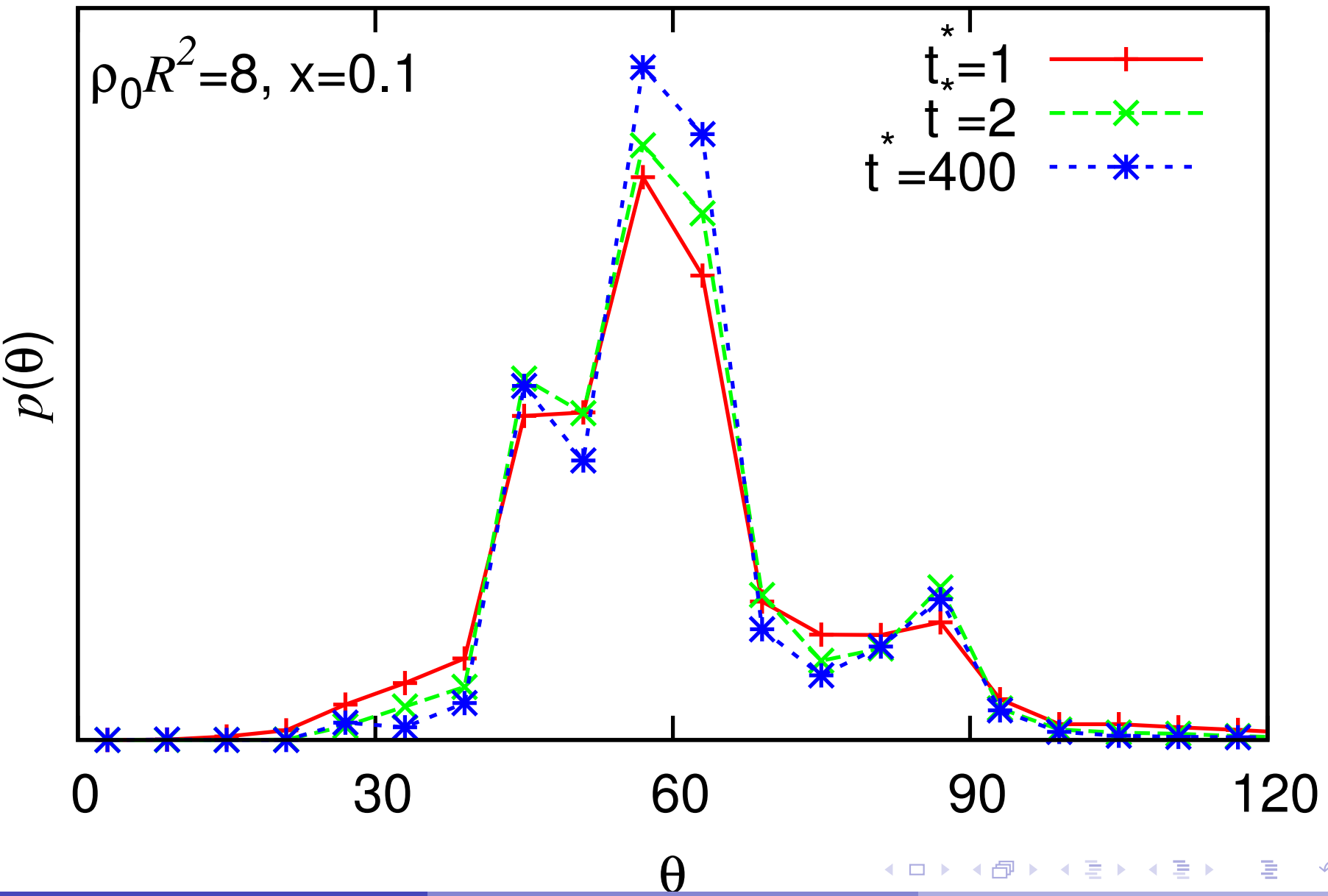

Speed of the solidification front in 2D

How good is this type of theory? The amplitude equations predict:

$$\gamma_{\mathrm{M}} = -\frac{2}{9(1+2\lambda)} \qquad \gamma_{\mathrm{sn}} = -\frac{1}{4(1+2\lambda)},$$

i.e., $\gamma_{\mathrm{M}}/\gamma_{\mathrm{sn}} = 8/9$. From the simulations of the GEM-4 front we have

$$\beta\mu_{\mathrm{sn}} \approx 16.5 \quad \text{and} \quad \beta\mu_{\mathrm{M}} \approx 16.8,$$

while the linear instability threshold corresponds to $\beta\mu_{\mathrm{lin}} \approx 19.6$. Thus $(\mu_{\mathrm{M}} - \mu_{\mathrm{lin}})/(\mu_{\mathrm{sn}} - \mu_{\mathrm{lin}}) \approx 0.90$, very close to the predicted value $8/9$.
But all is not well. The amplitude equations also predict that $|\gamma_{\mathrm{M}}|/\gamma_1 \approx 2.5$ over the entire range of nonlinear coefficients λ while simulations indicate that $|\gamma_{\mathrm{M}}|/\gamma_1 \approx 1.4$.
The possible sources of discrepancy are:

- Absence of pinning between the first front and the stripes, and between the second front and the hexagons/stripes
- Absence of the long wave mode arising from particle number conservation

Conclusions

We have shown that the speed of crystallization fronts can be computed within both

- PFC model
- DDFT

and discussed the differences between the corresponding behavior in one and two spatial dimensions. We have shown that a moving front selects a nonequilibrium wavelength and hence that front propagation leads to a state that must undergo glass-like behavior as it seeks to find local thermodynamic equilibrium after the passage of the front, at least for sufficient supercooling. The results can be interpreted within appropriate theory describing front propagation in 1D and 2D.

References:
Archer et al., Phys. Rev. E **86**, 031603 (2012)
Thiele et al., Phys. Rev. E **87**, 042915 (2013)
Archer et al., Phys. Rev. E **90**, 042404 (2014) and in press